Doctorate Dissertation
博士論文

Selective trans-omic regulation of insulin action by its doses across the multiple-omic layers

(多階層オミクスデータを用いたインスリン濃度に対する
細胞内情報伝達ネットワーク選択性の解明)

A Dissertation Submitted for Degree of Doctor of Philosophy

submitted on 08/2018

平成 30 年 8 月 博士 (理学) 申請

Department of Biological Sciences, Graduate School of Science,
The University of Tokyo
東京大学大学院理学系研究科生物科学専攻

Kentaro Kawata
川田 健太郎

Abstract

Insulin selectively regulates multiple cellular functions such as gene expression and metabolism by its doses and temporal patterns. However, the global network that underlies insulin action and selective use of specific pathways by dose and time remain unknown. Here we reconstructed global trans-omic network of insulin action using phosphoproteome, transcriptome, and metabolome data. We first reconstructed trans-omic networks; including phosphorylation-dependent cellular functions regulatory network, transcriptional regulatory network, phosphorylation- and allostery-dependent metabolism regulatory network. We integrated these trans-omic networks, and obtained the trans-omic regulatory network. Further, we identified selective regulatory network by dose and time of insulin. Akt and Erk encode information of a wide dynamic range of insulin. Down-regulated genes and metabolites in glycolysis show high sensitivity and fast response, and up-regulated genes and dicarboxylic acids in TCA cycle show low sensitivity and slow response, indicating that these downstream effectors selectively decode information of dose and time of insulin.

Table of Contents

1. Abbreviations

Abbreviations	Full Spellings
[Proteins]	
Acaca	acetyl-CoA carboxylase alpha
Acly	ATP citrate lyase
Ampk	adenosine monophosphate-activated protein kinase
Creb	cAMP response element-binding protein
Egr1	early growth response 1
eIf4b	eukaryotic translation initiation factor 4B
eIf4ebp1	eukaryotic translation initiation factor 4E-binding protein 1
Erk1	extracellular signal–regulated kinases 1
Erk2	extracellular signal–regulated kinases 2
Fasn	fatty acid synthase
Grb2	growth factor receptor-binding protein 2
Gsk3β	glycogen synthase kinase 3β
Hes1	hairy and enhancer of split-1
InsR	insulin receptor
Irs1	insulin receptor substrate 1
Irs2	insulin receptor substrate 2
Jnk	c-Jun N-terminal kinase
mTORC1	mTOR complex 1
Pfkfb	6-phosphofructo-2-kinase/fructose-2,6-biphosphatase 1
Pfkl	phosphofructokinase, liver type
PI3k	phosphatidylinositol 3-kinase
S6k	S6 kinase
Tsc1	tuberous sclerosis 1
Tsc2	tuberous sclerosis 2
[Genes]	
G6Pase	*glucose-6-phosphatase*
Pck1	*phosphoenolpyruvate carboxykinase1*

Abbreviations	Full Spellings
[Amino acids]	
Ser	serine
Thr	threonine
Tyr	tyrosine
[Methods]	
CE-TOFMS	capillary electrophoresis time-of-flight mass spectrometry
MRM	multiple reaction monitoring
PBS	phosphate-buffered saline
[Statistics]	
ANOVA	analysis of variance
AUC	area under the curve
SEM	standard error of the mean
[Others]	
DCM	differentially changed metabolite
DEG	differentially expressed gene
DET	differentially expressed transcript
FPKM	fragments per kilobase of transcript per million mapped reads
IRpP	insulin-responsive phosphopeptide
KSR	kinase-substrate relationship
PPI	protein-protein interaction
RME	responsible metabolic enzyme
RPK	responsible protein kinase
TF	transcription factor
TFBM	transcription factor binding motif

2. Introduction

2.1 Insulin signaling

The recent increase in metabolic disorders related to insulin resistance is a major health concern [1]. Understanding how cells interpret this physiologically dynamic hormone may provide new insights into preventing or treating metabolic disorders associated with insulin resistance. Insulin regulates systemic metabolic homeostasis via multiple regulation, including metabolism, gene expression, and protein synthesis. Liver, skeletal muscle, and adipose tissue are known as the target tissues of insulin [2–4]. In the liver, insulin signal is transmitted through signaling pathway via activation of insulin receptor (InsR) [3,5]. The activated InsR triggers series of phosphorylations in signaling pathway including insulin receptor substrate 1 and 2 (Irs1 and Irs2), Akt, mTOR complex 1 (mTORC1), extracellular signal–regulated kinases 1 and 2 (Erk1 and Erk2), p38, and adenosine monophosphate-activated protein kinase (Ampk), and multiple cellular functions are regulated through the phosphorylations of specific target molecules [3,5–8]. Insulin also regulates gene expression through mainly Akt signaling pathway and Mapks (Erk and p38) signaling pathway [3,5,9–11]. Akt directly phosphorylates Foxo family of forkhead

transcription factors (TFs) including Foxo1 (also known as Fkhr), leading to nuclear exclusion of Foxo1 [12,13]. The exclusion of Foxo1 suppresses gluconeogenesis by reducing the expression of *glucose-6-phosphatase* (*G6Pase*) and *phosphoenolpyruvate carboxykinase1* (*Pck1*), which are rate-limiting enzymes of gluconeogenesis [3,14]. Erk regulates gene expression through activation of cAMP response element-binding protein (Creb) and induction of TFs such as early growth response 1 (Egr1), and hairy and enhancer of split-1 (Hes1) [15–18]. Insulin also activates c-Jun N-terminal kinase (Jnk) via phosphatidylinositol 3-kinase (PI3k) and growth factor receptor-binding protein 2 (Grb2), and activates TFs such as c-Jun and activating transcription factor 2 (Atf2) through phosphorylations [19,20]. global metabolism such as glycolysis/gluconeogenesis, glycogenesis, amino acids, and lipid metabolism are regulated through series of phosphorylations of metabolic enzymes by signaling molecules such as glycogen synthase kinase 3β (Gsk3β), allosteric regulation and gene expression [2]. Moreover, insulin also regulates proteins synthesis by phosphorylation of ribosomal protein S6 kinase (S6k) that phosphorylates ribosomal protein S6, eukaryotic translation initiation factor 4E-binding protein 1 (eIf4ebp1), and eukaryotic translation initiation factor 4B (eIf4b) via mTORC1 phosphorylated and activated by Akt through tuberous sclerosis 1 and 2 (Tsc1 and Tsc2)

[6,21,22]. Additionally, insulin regulates other cellular functions such as cell adhesion, cytoskeleton, and splicing [23–26]. These cellular functions are coordinately regulated by insulin signal transmitted across large-scale network consisting of protein phosphorylations, metabolites, mRNAs, and protein synthesis. However, how insulin globally regulates protein phosphorylation, gene expression, metabolism, protein synthesis, and other cellular functions has yet to be uncovered.

2.2 Developments of omic measurements

Recent Technical advances in phosphoproteomic, transcriptomic and metabolomic measurements enable us to large-scale quantitative analysis of changes in protein phosphorylation, gene expression, and metabolite abundance. For example, phosphoproteomic studies of insulin signaling have been demonstrated in 3T3-L1 mouse adipocytes [22], *Drosophila* cells [27,28], mouse hepatoma cells [29], rat primary hepatocytes [30], mouse brown preadipocytes [31], and rat FAO hepatoma cells [32]. Transcriptomic studies of insulin signaling have been demonstrated in rat hepatoma cells [33], mouse fibroblasts [34,35], mouse osteoclast precursors [36], and human skeletal muscle [37]. Sano *et al*. also previously analyzed gene expression using transcriptome data

in insulin-stimulated FAO cells [38]. Metabolomic studies of insulin signaling have been demonstrated in human [39], human plasma [40], and rat FAO hepatoma cells [32,41]. Despite such progress in each omic layer analysis of insulin action, little has been reported for interactions between the multi-omic layers [42–46].

2.3 Developments of multiple omic analysis

We have recently proposed “trans-omics” as a discipline for reconstructing molecular interaction across multiple omic layers based on direct molecular interactions rather than indirect statistical relationship [32,47,48]. Recently, trans-omic analyses of global networks of metabolic control have been reported in metabolic control in *Escherichia coli* [49,50], in *Bacillus subtilis* [42], in *Saccharomyces cerevisiae* [51–53], in Chinese hamster ovary cells [54], and in human T-cell [55]. Yugi *et al*. have previously reconstructed trans-omic networks regulating metabolism through phosphorylation by acute insulin action using phosphoproteome and metabolome data [32]. However, the network regulating other cellular functions via protein phosphorylation, gene expression, protein synthesis, and metabolism remains to be clarified.

2.4 Selectivity of the intracellular molecules against insulin temporal patterns

Temporal patterns of specific growth factors coding extracellular information are encoded into signaling pathways, and are selectively decoded by distinct downstream molecules by differences in the sensitivities, time constants, and network structures [56]. Secretion of insulin show distinct temporal patterns in response to blood glucose level: transient additional secretion at a high dose and sustained basal secretion at a low dose [57,58]. We previously demonstrated that signal molecules, metabolites, and gene expression, show distinct sensitivity and rate response against insulin, selectively responding to additional and basal secretion of insulin. Phosphorylations of S6k and Gsk3β, insulin signaling factors, showed low sensitivity and fast response, responding to additional secretion of insulin, while *G6pase* showed high sensitivity and slow response, responding to basal secretion [59]. F1,6BP, a central metabolites of glycolysis, and glycogen showed low sensitivity fast response, responding to additional secretion, while Pck1 showed high sensitivity and slow response, responding to basal secretion [41]. Up-regulated genes by insulin show low sensitivities and fast responses, responding to additional secretion, while down-regulated genes show high sensitivities and slow responses, responding to basal secretion of insulin

[38]. However, the overview of selectivity of the whole molecules in the trans-omic network by doses and temporal patterns of insulin has yet to be demonstrated.

2.5 Purpose of this study

In this study, I reconstructed trans-omic network using phosphoproteome, transcriptome, and metabolome data in insulin-stimulated FAO cells. First, a trans-omic regulatory network comes across three omic layers, phosphoproteome, transcriptome, and metabolome, was reconstructed. The trans-omic regulatory network includes three subnetworks: phosphorylation-dependent cellular functions regulatory network; transcriptional regulatory network via TFs; phosphorylation- and allostery-dependent metabolism regulatory network. Then, I estimated sensitivities and time constants of signaling molecules, gene expression, and metabolism against insulin stimulation, and identified selectivity of the molecules by dose and time of insulin, reflecting the selective use of specific pathways by additional and basal insulin secretion. This study demonstrates the trans-omic regulatory network of insulin action that realizes physiological modes of action, based on phosphoproteome, transcriptome and metabolome.

3. Results

3.1 Reconstruction of the trans-omic regulatory network of insulin action

In this study, I reconstructed trans-omic network of chronic insulin action in rat FAO hepatoma cells by integrating phosphoproteome, transcriptome, and metabolome data. In the previous study, Yugi *et al*. reconstructed a trans-omic network of acute insulin action (< 60 min) in rat FAO cells via mainly phosphorylation, based on metabolome and phosphoproteome data [32]; however, transcriptional regulation, as well as phosphorylation, is related to metabolism regulation in chronic insulin action, and insulin regulates not only metabolism but also various cellular functions such as cell adhesion, cytoskeleton, and splicing [23–26]. Therefore, I reconstructed global trans-omic network of insulin action in FAO cells including protein phosphorylation, gene expression, enzymatic regulation, and allosteric regulation by integrating phosphoproteome, transcriptome and metabolome data obtained from insulin-stimulated Fao cells. This reconstruction of the trans-omic regulatory network was performed by the following four steps (Fig. 1): Step I, reconstruction of phosphorylation-dependent regulatory network regulating cellular functions (cellular functions regulatory network) based on phosphoproteome data; Step II, reconstruction of

transcriptional regulatory network via TFs (transcriptional regulatory network) based on transcriptome and phosphoproteome data; Step III, reconstruction of phosphorylation- and allostery-dependent network regulating metabolism (metabolism regulatory network) based on metabolome and phosphoproteome data; Step IV, reconstruction of global regulatory network (trans-omic regulatory network) by integrating the regulatory networks reconstructed in Steps I to III. I further identified selective regulation of the molecules in the trans-omic regulatory network by dose and time of insulin by estimating sensitivities and time constants against insulin stimulation.

3.2 Step I: Reconstruction of cellular functions regulatory network

Insulin binds to the receptor to trigger series of phosphorylations in signaling pathways such as PI3k-Akt signaling pathway and Mapk signaling pathway [3,5–8]. These phosphorylations are transmitted through intracellular signaling networks to regulate multiple cellular functions. In this step, I reconstructed cellular functions regulatory network, which transmits insulin signal via mainly phosphorylation to regulate cellular functions, based on phosphoproteome data. The cellular functions regulatory network was

reconstructed in the three substeps: (i) identification of signaling layer transmitting insulin signal, (ii) identification of insulin-dependent phosphorylations on cellular functions, and (iii) estimation of the responsible protein kinases of the insulin-responsive phosphopeptides (IRpPs).

3.2.1 Identification of the signaling layer

In the previous study, Yugi *et al*. analyzed the phosphoproteome data of acute insulin action [32]. However, among the detected phosphopeptides, only a part of phosphopeptides on the metabolic enzymes has been considered in the previous study. In this study, I utilized all of the phosphopeptides detected in the phosphoproteome data for the reconstruction of trans-omic network. The phosphoproteome data detected 7,929 phosphopeptides derived from 3,468 proteins, including 6,989 phosphoserine (pSer), 1,421 phosphothreonine (pThr), and 79 phosphotyrosine (pTyr) (Fig. 2a). Note that since some of the phosphopeptides have multiple phosphorylated residues, the sum of the numbers of the phosphorylated residues is not equal to the number of phosphopeptides. Singly phosphorylated peptides occupied 93.16% of all the 7,929 phosphopeptides (Fig. 2a). The distribution of phosphorylated sites by amino acid was consistent with the previous studies [22,60–62].

From the phosphoproteome data, the 3,288 IRpPs were identified (see Experimental Procedures), and the 1,947 proteins including at least one IRpP was defined as a differentially phosphorylated protein. The over-representation analysis with the differentially phosphorylated proteins on the signaling pathways (see Experimental Procedures) was performed to identify the 14 signaling pathways on which the differentially phosphorylated proteins were significantly over-represented (Fig. 2b; Table 1 and S1). The signaling layer transmitting insulin signaling by mainly phosphorylation was reconstructed by integration of the 14 signaling pathways (Fig. 2c). The signaling layer consists of 146 proteins and 19 compounds, and the proteins included in the signaling layer are defined as signaling factors. The signaling factors included well-known insulin-responsive signaling molecules such as Akt, Erk1, Erk2, and mTORC1 [3,5,14]. Among the 289 phosphopeptides derived from 125 signaling factors, 134 phosphopeptides indicated quantitative changes (56 increased, 43 decreased, and 33 increased and decreased). In the previous study, Yugi *et al*. used a part of rat *Insulin signaling pathway* (rno04910) from Kyoto Encyclopedia of Genes and Genomes (KEGG) database including 42 proteins and three compounds as a signaling layer [32]. Among the 42 proteins included in the previous signaling layer, 40 proteins (95.24%) except the molecules not being the

downstream of InsR such as Ship2 and Lar were also included in the signaling layer defined in this study, and 106 proteins were newly included.

3.2.2 Identification of cellular functional layer

To identify the insulin dependent cellular functions regulated via phosphorylation, the over-representation analysis with the differentially phosphorylated proteins on the cellular functional pathways, which are the KEGG pathways except for signaling pathways and the pathways that work in specific tissues other than liver (Table S2, see Experimental Procedures), was performed to identify the 11 cellular functional pathways on which the differentially phosphorylated proteins were significantly over-represented (Fig. 2d; Table 2 and S1). These cellular functional pathways were defined as cellular functional layer. The cellular functional layer included the pathways regulating cell adhesion such as *Tight junction* (rno04530) and *Gap junction* (rno04540), the pathways regulating cytoskeleton such as *Regulation of actin cytoskeleton* (rno04810), and the pathways regulating post-transcriptional regulation such as *RNA transport* (rno03013) and *Spliceosome* (rno03040).

3.2.3 Estimation of kinases regulating the IRpPs

To examine the regulation of the insulin-dependent cellular functions, the responsible protein kinases (RPKs) for the IRpPs in the pathways on the cellular functional layer were estimated using NetPhorest, a kinase-substrate relationship (KSR) estimation tool [63,64]. NetPhorest estimates posterior probabilities that a particular protein kinase classifier, including multiple kinases (Table S3), recognizes an amino acid residue. The kinases in the classifier indicating the largest posterior probability value was defined as RPKs (see Experimental Procedures). The cellular functional layer included 1,103 phosphopeptides and 492 IRpPs derived from 216 proteins. I estimated the 1,688 KSRs between 86 RPKs and 486 IRpPs in the cellular functional layer (Table S4).

To examine the selective usage of protein kinases for the insulin-dependent cellular functions, occurrence ratio of the RPKs in the 11 pathways in the cellular functional layer and metabolic enzymes identified from KEGG database was calculated (Table S5, see Experimental Procedures), and the pathways with the metabolic enzymes were hierarchically clustered by the occurrence ratios (Fig. 3a). The clustering analysis divided the pathways with the metabolic enzymes into two clusters. Cluster 1 included pathways regulating cell adhesion and cytoskeleton such as *Tight junction* (rno04530), *Gap junction*

(rno04540), and *Regulation of actin cytoskeleton* (rno04810), while cluster 2 included pathways regulating post transcription regulation such as *RNA transport* (rno03013) and *Spliceosome* (rno03040). In addition, to examine the protein kinases regulating the pathways included in each cluster, the motif logos of amino acid sequences of IRpPs in each pathway were generated by using enoLOGOS [65] (Fig. 3b). Many of logos generated against the pathways in cluster 1 had one arginine residue (R) at -3 position, suggesting that many of the pathways related to cell adhesion and cytoskeleton were regulated by the basophilic kinases such as Akt and Pka. While, many of logos generated against the pathways in cluster 2 had one proline residue (P) at +1 position, suggesting that many of the pathways related to post transcriptional regulation were regulated by the proline directed kinases such as Mapk. To examine these suggestions statistically, the amino acid compositions at each position of the IRpPs included in the pathways in cellular functional layer and metabolic enzymes, or each cluster were tested using iceLogo [66] (Fig. 3c). On the IRpPs in the cellular functional layer with the metabolic enzymes, one P at +1 position and one R at -3 position were significantly over-represented ($p < 0.05$). On cluster 1, except for valine residue (V) at +1 position, any amino acids residue were not significantly over-represented at all positions, and P at

+1 position significantly under-represented, while, on cluster 2, the P at +1 position was significantly over-represented. These results indicates that the phosphorylations in response to insulin were regulated by basophilic kinases such as Akt and Pka, and proline directed kinases such as Mapk, and especially, those in the pathways in cluster 2, such as post-transcriptional regulation, were regulated specifically by proline directed kinases.

The 28 RPKs among the estimated 86 RPKs were included in the signaling layer. The signaling layer and the cellular functional layer were connected by the 620 KSRs including the RPKs included in signaling layer and 186 IRpPs in the cellular functional layer. Thus, the cellular functions regulatory network was reconstructed (Fig. 4).

3.3 Step II: Reconstruction of transcriptional regulatory network

Insulin regulates gene expression, as well as phosphorylation, to regulate cellular functions including metabolism [2,3,5–8,21–26]. In the previous study, Sano *et al*. revealed that up-regulated and down-regulated genes in response to insulin stimulation exhibit different sensitivities and time constants, based on the transcriptome data [38]. The sensitivities are the time constants revealed to be important factors to determine selectivity against temporal patterns of insulin [59]. Therefore, in this study, I reconstructed a transcriptional regulatory

network regulating the genes indicating fast or slow time constants and high or low sensitivities via TFs (transcriptional regulatory network), based on the transcriptome and the phosphoproteome data. The transcriptional regulatory network was reconstructed in the four substeps: (i) identification of up-regulated and down-regulated differentially expressed genes (DEGs) by insulin stimulation; (ii) classification of the up-regulated and down-regulated DEGs according to the sensitivity (EC_{50}) and time constant ($T_{1/2}$); (iii) estimation of TFs specific to each class of DEGs; and (iv) identification of regulatory signaling factor for each TF.

3.3.1 Identification of up-regulated and down-regulated DEGs

Among all genes corresponding to the 490 differentially expressed transcripts (DETs) identified in the previous study [38], 433 genes detected at all time points were defined as the DEGs in this study. The DEGs were categorized into 114 up-regulated, 144 down-regulated, and 175 other DEGs according to the parameter indicating variation and area under the curve (AUC) ratios in each DEG (Fig. 5a and b; Table S6, see Experimental Procedures).

3.3.2 Classification of the up-regulated and down-regulated DEGs

I defined EC_{50} and $T_{1/2}$ values as parameters of sensitivity against insulin doses and that of time constant in response to insulin stimulation, respectively (Fig. 5c, see Experimental Procedures). EC_{50} was defined as the dose of insulin that provides the 50% of the maximal AUC of time series of gene expression. The smaller EC_{50} indicates the higher sensitivity to insulin dose, and vice versa. $T_{1/2}$ was defined as the time when the response reaches 50% of the peak amplitude. The smaller $T_{1/2}$ indicates the faster response, and vice versa. The EC_{50} and $T_{1/2}$ values were calculated for each of up-regulated or down-regulated DEGs. The distributions of both of EC_{50} and $T_{1/2}$ values between the up-regulated and down-regulated DEGs were significantly different (adjusted $p < 0.01$), and the averages of EC_{50}s and $T_{1/2}$s of the up-regulated DEGs were lager and smaller than those of the down-regulated DEGs, respectively (Fig. 5d; Table 3), consistent with the previous observation [38]. For the EC_{50} and $T_{1/2}$ values, I determined the thresholds dividing the distributions into large and small values (θ_1 for EC_{50}, and θ_2 for $T_{1/2}$). The up-regulated and down-regulated DEGs were classified into four classes according to the thresholds (Fig. 5e and 11b; Table S6, see also Fig. 11b): Class 1, high sensitivity ($EC_{50} < \theta_1$) and fast response ($T_{1/2} < \theta_2$); Class 2, high sensitivity and slow response ($T_{1/2} > \theta_2$); Class 3, low sensitivity ($EC_{50} > \theta_1$) and fast

response, and Class 4, low sensitivity and slow response. The majority of the up-regulated DEGs (57 out of 114 up-regulated DEGs) belongs to Class 3 (low sensitivity and fast response), and that of the down-regulated DEGs (70 out of 144 down-regulated DEGs) belongs to Class1 (high sensitivity and fast response).

3.3.3 Estimation of TFs specific to each class of DEGs

The TFs specific for the classes of up-regulated and down-regulated DEGs were estimated using TRANSFAC [67] and Match, a TF binding motifs (TFBMs) estimation tool [68], and motif enrichment analysis (Fig. 6a; Table S7, see Experimental Procedures). Twenty-two and 12 TFs were estimated for the classes of up-regulated DEGs and those of down-regulated DEGs, respectively, and these were mutually exclusive except for Foxo1. The TFs specific for the classes of the up-regulated DEGs included the well-known insulin-responsive TFs such as Creb, Srf, and Egr1 [15–18]. Foxo1, that is also known as a well-known insulin-responsive TFs [12,13], was estimated in common for all classes of down-regulated DEGs and for Class 4 of the up-regulated DEGs.

3.3.4 Identification of regulatory signaling factor for each TF

To identify the regulation against the estimated TFs, the intracellular molecules regulating the activities of the estimated TFs were identified from KEGG database (Table S8). The 117 proteins regulating the 12 out of the estimated 33 TFs were identified, defined as regulators. Among the 117 regulators, 56 regulators related to 10 TFs were included in the signaling layer. The 10 TFs were connected to the 56 out of identified 117 regulators in the signaling layer to reconstruct the transcriptional regulatory network (Fig. 6b).

Estimation of TFs for the up-regulated and down-regulated DEGs reveals the selective regulation of the DEGs by different TFs sets. The TFs estimated for the up-regulated DEGs include Egr1, Creb1, and Srf, while those for the down-regulated DEGs include Foxo1. Given that activations of the former TFs have been regulated mainly by Erk/Mapk pathways [15–18], while activation of Foxo1 is regulated by Akt pathway [9,10,69,70], the up-regulated DEGs are likely to be regulated by Erk/Mapk pathways, while the down-regulated DEGs by Akt pathways.

3.4 Step III: Reconstruction of metabolism regulatory network

In the previously study, Yugi *et al*. reconstructed phosphorylation-dependent metabolic regulatory network of acute insulin action (< 60 min) based on metabolome and phosphoproteome data [32]. In this study, I reconstructed phosphorylation-dependent metabolic regulatory network of chronic insulin action (< 240 min) (metabolism regulatory network) based on the metabolome and the phosphoproteome data. The metabolism regulatory network was reconstructed in the three substeps: (i) identification of differentially changed metabolites (DCMs) and their responsible metabolic enzymes (RMEs); (ii) identification of allosteric regulation of RMEs by DCMs; and (iii) estimation of the RPKs of the IRpPs in RMEs. Note that since many of protein phosphorylations by insulin stimulation change sufficiently up to 60 min (see also Fig. 10), the acute phosphoproteome data utilized in previous study [32] was also used for reconstruction of the metabolism regulatory network.

3.4.1 Identification of DCMs and their RMEs

Based on the metabolome data of chronic insulin action (< 240 min), the 93 metabolites whose abundances were significantly changed by insulin stimulation were identified and

defined as differentially changed metabolites (DCMs) (Table S10, see Experimental Procedures). Among the 93 DCMs, I identified 42 increased and 43 decreased DCMs in the same manner with the DEGs. In the central carbon metabolism, DCMs in the upstream of glycolysis (G6P and F6P) decreased, while DCMs in the downstream of glycolysis (F1,6BP, 3PG, and PEP) and those in the TCA cycle (Citrate, 2-Oxoglutarate, Succinate, Fumarate, and Malate) increased (Fig. 7a and b). Many amino acids decreased, while Ala, Arg, and Ser increased (Fig. 7a). Yugi *et al*. identified 55 metabolites quantitatively changed in respond to acute insulin action [32], and 27 of which (49.09%) were included also in the DCMs (Fig. 7c). The differences may be partly due to the difference of insulin stimulation time and definition of changed metabolites.

Abundances of metabolites change depending on the reaction rates of the production (influx) and consumption (efflux) that are determined by modification of enzymes, amounts of enzyme, and amounts of substrate and product. Hereafter, the metabolic enzymes that directly produce or consume at least one DCM were defined as RMEs. The 283 RMEs for 62 out of the 93 DCMs were identified from the KEGG database (Fig. 7d; Table S11). In the previous study, Yugi *et al*. identified 198 metabolic enzymes regulating metabolites changed quantitatively in respond to acute insulin action [32], and 123 of which (62.12%)

were included also in the RMEs defined in this study (Fig. 7c). The differences may be partly due to the difference of insulin stimulation time and definition of DCMs.

3.4.2 Identification of allosteric regulation of RMEs by DCMs

Since some kinds of metabolites activate or inhibit metabolic enzymes as allosteric effectors, the DCMs functioning as allosteric effectors of each RME were identified from BRENDA database, a database providing information regarding allosteric effectors and their target enzymes from a comprehensive literature search [71] (Fig. 7e; Table S12). Among the 93 DCMs, 70 DCMs were identified as allosteric effectors for the 146 RMEs via a total of 381 allosteric regulations. An allosteric effector can operates as an activator for some enzymes and as an inhibitor for others. The identified 70 allosteric effectors were related to the 146 RMEs via 83 activations and 323 inhibitions.

3.4.3 Estimation of the RPKs of the RMEs

Phosphorylations of metabolic enzymes can regulate the enzymatic activity of the RMEs. I examined the phosphopeptides included in the RMEs from the phosphoproteome data, and identified 174 phosphopeptides derived from 51 RMEs. Among 174 phosphopeptides, 77 phosphopeptides derived from 30 RMEs, corresponded to 29 DCMs, were included in the

IRpPs (Table S11). The 54 RPKs regulating the 127 IRpPs among those in the RMEs via 106 KSRs, were estimated using NetPhorest (Table S1). In the previous study, Yugi *et al*. estimated 71 KSRs between 13 RPKs and 106 IRpPs that belong to 26 RMEs [32]. Twenty out of the 26 phosphorylated enzymes were included in the 30 phosphorylated RMEs in this study (Fig. 7c). The difference may be partly due to the differences of the DCMs.

The RPKs in signaling layer were connected to the IRpPs in the RMEs via the estimated KSRs. Among the 54 RPKs in 106 KSRs, 18 RPKs in 19 KSRs were included in the signaling layer, and were connected to 10 RMEs. Thus, the metabolism regulatory network regulating metabolism via 19 KSRs estimated between the 18 RPKs and 10 RMEs, 395 enzymatic regulations by 283 RMEs against the 62 DCMs, and 381 allosteric regulations (83 activations and 323 inhibitions) by 70 DCMs against the 146 RMEs, were reconstructed (Fig. 8).

3.5 Step IV: Reconstruction of trans-omic regulatory network

The cellular functions regulatory network (Fig. 4), the transcriptional regulatory network (Fig. 6b), and the metabolism regulatory network (Fig. 8) were integrated to reconstruct a

trans-omic regulatory network. Since these networks includes a common signaling layer, the downstream of signaling layer such as cellular functional layer, TFs, and RMEs were connected to single signaling layer. Moreover, since the reaction rates of influx and efflux that change the abundance of the metabolites are determined by amounts of the enzyme as well as the modifications of the metabolic enzymes such as allosteric regulation and phosphorylation, five DEGs coding RMEs were identified from the transcriptome data (Table S11). Herewith, the trans-omic regulatory network regulating cellular functions including metabolism via protein phosphorylation, transcription, enzymatic regulation, and allosteric regulation were reconstructed (Fig. 9).

In the trans-omic regulatory networks, the RMEs were regulated by three different modules; protein phosphorylation, gene expression, and allosteric regulation. Among 283 RMEs, 30 RMSs were differentially phosphorylated, and 10 of which are connected to kinases in the signaling layer. The differentially phosphorylated RMEs include 6-phosphofructo-2-kinase/fructose-2,6-biphosphatase 1 (Pfkfb) and phosphofructokinase, liver type (Pfkl), which are rate-limiting enzymes of glycolysis/gluconeogenesis, ATP citrate lyase (Acly), acetyl-CoA carboxylase alpha (Acaca), and fatty acid synthase (Fasn), which are rate-limiting enzymes of fatty acid synthesis. Five up-regulated or

down-regulated DEGs cording the RMEs such as *G6Pase* and *Pck1*, rate-limiting enzymes of gluconeogenesis, were identified. Moreover, the 70 out of 93 DCMs were identified as allosteric effectors.

Numbers of protein phosphorylations and gene expression for RMEs were limited compared with those of allosteric regulation. This characterizes the metabolic regulations by protein phosphorylation, gene expression and allosteric regulation. Primarily, insulin acts only on a few but key regulatory points in the metabolic pathway such as the rate-limiting enzymes via protein phosphorylation and gene expression. This primary metabolic regulation on the few regulatory points are rapidly transmitted to numerous metabolites along with metabolic pathways, thereby change considerable numbers of allosteric effectors that work as secondary regulators of insulin signal to more metabolic enzymes than the primary regulation.

3.6 Elucidation of selectivity of the trans-omic regulatory network to insulin doses

Insulin exhibits specific temporal patterns by dose and time; basal secretion, which is a low dose secretion with slow and sustained temporal pattern during fasting, and additional

secretion, which is a high dose secretion with rapid and transient increase in response to meals *in vivo* [57] (Fig. 10a left). To examine which the individual molecules in the trans-omic regulatory network respond selectively to additional or basal secretion of insulin, I attempted to identify selective regulation of the molecule by dose and time of insulin, according to the EC_{50} and the $T_{1/2}$ values. The molecules indicating smaller $T_{1/2}$ respond to insulin stimulation faster, while those indicating larger $T_{1/2}$ respond slower. Since the molecules indicating small EC_{50} saturate with low insulin dose, tending to be indistinguishable between low and high dose of insulin, while since those indicating large EC_{50} differently respond to low and high dose of insulin, tending to be distinguishable the dose of insulin stimulation (Fig. 10a right).

The parts of molecules in signaling layer, transcription factors, and protein synthesis related factors were classified into four classes, as well as the classification of the DEGs, according to their EC_{50} and $T_{1/2}$ values. Within the molecules in signaling layer, Hatano measured phosphorylations of Irs1 (pIrs1), Akt (pAkt), S6k (pS6k), Gsk3β (pGsk3β), Erk (pErk), p38 (pp38), Jnk (pJnk), Ampk (pAmpk), and Tsc2 (pTsc2) in time series by western blotting (Fig. 11). Within the transcription factors, Hatano measured phosphorylations of Foxo1 (pFoxo1), Creb (pCreb), Atf2 (pAtf2), and c-Jun (pc-Jun),

and protein abundances of Egr1, c-Jun, and Hes1 in time series by western blotting (Fig. 11). Within the protein synthesis related factors, Hatano measured phosphorylations of S6 (pS6), eIf4ebp1 (peIf4ebp1), and eIf4b (peIf4b) in time series by western blotting (Fig. 11). Hereafter, these molecules measured by western blotting were denoted as signaling molecules. The EC_{50} and the $T_{1/2}$ values of the signaling molecules were calculated from the western blotting data, and the signaling molecules were classified into four classes according to their EC_{50} and $T_{1/2}$ values, in same manner with the DEGs (Fig. 10b left; Table S13, see Experimental Procedures).

The increased and decreased DCMs were also classified into four classes, as well as the classification of the DEGs and the signaling molecules. The EC_{50} and the $T_{1/2}$ values were calculated based on the metabolome data. Distributions of both of EC_{50}s and $T_{1/2}$s between the increased and decreased DCMs were significantly different (adjusted $p < 0.01$), and both of the averages of EC_{50}s and $T_{1/2}$s of the increased DCMs were larger than those of the decreased DCMs (Fig. 10b right; Table 4). Furthermore, both of the distribution of EC_{50}s of the increased and decreased DCMs looked unimodal. The distribution of $T_{1/2}$s of the DCMs looked bimodal, while that of the decreased DCMs looked unimodal. According to the EC_{50}

and $T_{1/2}$ values, the DCMs were classified into four classes, in same manner with the DEGs and the signaling molecules (Fig. 10b right; Table S10, see Experimental Procedures).

The thresholds of EC_{50} values for the signaling molecules, the DEGs, and DCMs were 0.63 nM, 0.70 nM, and 0.40 nM, respectively, indicating that the threshold of EC_{50}s are within the similar range of sub nanomolar order. It is noteworthy that the estimated thresholds of EC_{50}s were within sub nanomolar order, corresponding to the insulin dose distinguishing between additional secretion (nM order) and basal secretion (tens to hundreds of pM) [57,58] (Fig. 10b). The thresholds of $T_{1/2}$ values of signaling molecules, the DEGs, and DCMs are 36.21 min, 87.59 min, and 54.17 min, respectively (Fig. 10b), suggesting the delay from insulin-signaling to metabolism and to gene expression.

3.6.1 Selectivity of the signaling molecules

Within the signaling factors in signaling layer, pIrs1, pJnk, pAkt, and pErk show low sensitivity and fast response (Class 3), indicating that these hub molecules of insulin-signaling, can encode information of a wide dynamic range against dose and time of insulin across basal and additional secretion (Fig. 10b left; Table 13). On the other hand,

pS6k, pTsc2, pp38, and pGsk3β show high sensitivity and fast response (Class 1), indicating that these downstream effectors of the hub molecules are sensitive to low dose of insulin and are likely to selectively respond to basal secretion (Fig. 10b left; Table 13).

Within the TFs, pCreb and pFoxo1 were included in the TFs in Class 1 (high sensitivity and fast response), while Egr1 and Hes1 were included in those in Class 4 (low sensitivity and slow response) (Fig. 10b left; Table 13). The former, Creb and Foxo1, are regulated by phosphorylation by signaling factors including Erk and Akt [10,14,18,69], while the latter, Egr1 and Hes1, are regulated by gene expression [72–75]. Indeed, both *Egr1* and *Hes1* genes were included in the Class 1 of up-regulated DEGs (Fig. 10b middle; Table 13). The difference in the sensitivities and the time constants between pCreb and pFoxo1, and Egr1 and Hes1 are likely due to the different regulatory mechanisms, protein phosphorylation and gene expression, respectively.

Within the protein synthesis related factors, all of those measured in this study (pS6, peIf4ebp1, and peIf4b) were included in Class 1 (high sensitivity and fast response), indicating that protein synthesis reflects basal secretion of insulin in fasting state but not additional secretion in fed state (Fig. 10b left; Table 13).

3.6.2 Selectivity of the DEGs

For the DEGs classified above, majority of the down-regulated DEGs (Class 1 and 2) are mainly regulated in response to basal secretion of insulin, while that of the up-regulated DEGs (Class 3 and 4) are regulated in response to additional secretion (Fig. 10b middle; Table S6). The former includes, *G6Pase* and *Pck1*, the genes of rate-limiting enzymes of gluconeogenesis promoted in fasting state [3,14], while the latter includes *Hmgcr*, the gene of rate-limiting enzyme of cholesterol synthesis, promoted in the fed state [76,77], consistent with the physiological role of the DEG. Notably, among the up-regulated DEGs, the DEGs included in the class indicating low sensitivity and fast response (Class 3) are regulated by the Creb indicating fast response, while those included in the classes indicating slow response (Class 2 and 4) are regulated by the Hes1 and Egr1 indicating slow response, suggesting that the response rates of the up-regulated DEGs are affected by the activity rates of the transcription factors. Conversely, all down-regulated DEGs are regulated by Foxo1 indicating fast response, suggesting that the response rates of the down-regulated DEGs are affected by the degradation rates of individual genes.

3.6.3 Selectivity of the DCMs

For DCMs, those in upstream of glycolysis (F6P, F1,6BP, and DHAP) and downstream of glycolysis (3PG and PEP) are included in Class 1 and 2, respectively (Fig. 7a, 7b, and 10b right; Table S10). The DCMs in fatty acid synthesis (Citrate and Malonyl CoA) are included in Class 2. Considering that Class 1 and Class 2 are the classes of metabolites indicating high sensitivity with fast and slow response, respectively, upstream of glycolysis is primarily regulated by basal secretion of insulin, leading to subsequent changes in downstream glycolysis and fatty acid synthesis. Dicarboxylic acids in TCA cycle (Succinate, Fumarate, and Malate) are included in Class 4, regulated by additional secretion of insulin. These results indicate that the central carbon metabolism is divided into three functionally different blocks by dose and time of insulin; upstream of glycolysis, downstream of glycolysis and tricarboxylic acid in TCA cycle (Citrate), and dicarboxylic acids in TCA cycle (Succinate, Fumarate, and Malate). These results indicate that the pattern of insulin stimulation divides the central carbon metabolism into three functional blocks: (i) a block with metabolites that are upstream of glycolysis, (ii) a block with metabolites that are downstream of glycolysis and tricarboxylic acid in the TCA cycle, and (iii) dicarboxylic acids in TCA cycle.

For amino acid metabolism, most of the amino acids such as BCAAs are decreased in response to insulin stimulation, and included in the class indicating high sensitivity and fast response (Class 1), while a parts of the amino acids being proximal to central carbon metabolism such as Ala, Ser, Arg are increased in response to insulin stimulation, and included in the class indicating low sensitivity and slow response (Class 4) (Fig. 7a and 10b right; Table S10). This result indicates that the pattern of insulin stimulation divides amino acid metabolism into two functional blocks.

Thus, downstream effectors of insulin such as gene expression and metabolism can selectively decode information of dose and time of insulin. According to the dose and time of *in vivo* patterns of insulin secretion such as basal and additional secretions, I demonstrate the selective regulation in the global trans-omic network by dose and time of insulin. I extracted the molecules of the four classes of signaling molecules, the DEGs and the DCMs from the trans-omic regulatory network, and reconstructed the selective regulatory network according to sensitivities and time constants (Fig. 10c).

4. Discussion

In this study, I demonstrated a global trans-omic network reconstructed by integrating phosphoproteome, transcriptome, and metabolome data obtained from insulin-stimulated rat hepatoma FAO cells. Some major components for a trans-omics network such as expression proteome, protein-protein interactions (PPIs), fluxome, and epigenome are not included in this study. These components will be included for more complete pictures of a trans-omic network in the future study. Addition of expression proteome will provide further information such as regulation of protein expression, stoichiometry of protein phosphorylation, and comprehensive regulation of metabolic network. Correlation analysis between expression proteome and transcriptome will provide information of selective regulation of protein expression via transcription, translation, and protein degradation. Expression proteome data together with phosphoproteome data enables us to quantify stoichiometric changes of protein phosphorylation, and to clarify a comprehensive picture of metabolic regulation by changes of amounts of enzymes in addition to phosphorylations of enzymes and allosteric regulation by metabolites. Other modifications of proteome such as oxidation and acetylation of proteins will also be incorporated. The phosphoproteome

data with KEGG pathways were used for reconstruction of cellular functions, transcriptional, and metabolism regulatory networks; however, PPIs can provide the other regulations for these regulatory networks. Co-immunoprecipitation and proteomic measurement will provide comprehensive information of PPIs with key molecules, which will be included into a trans-omic network [27,28]. While The metabolome data, providing instantaneous information on metabolite concentrations, were used for reconstruction of metabolic regulation in this study, metabolism is a dynamic process, which is characterized by fluxes [42,49,51,78]. Addition of fluxome data will provide information of dynamics process of metabolism. Regulation of gene expression depends not only in transcriptional regulation by TFs, but also on epigenomic regulation such as DNA methylation and histone modifications [79–81], which will provide information of comprehensive picture of a gene expression regulatory network.

I also revealed the selectivity of the molecules in the trans-omic regulatory network by dose and time of insulin according to the EC_{50} and $T_{1/2}$ values. To avoid assumption of specific models, the EC_{50} and the $T_{1/2}$ values were calculated based on linearly complemented measurement data in this study. Therefore, the distributions of the EC_{50} and the $T_{1/2}$ values might be biased depending on the measured time points and doses of

insulin. Future developments of systematic understanding of the regulation of the molecules enable us to estimate sensitivities and time constants more properly. The EC_{50} and $T_{1/2}$ values were calculated based on the western blotting, the transcriptome, and the metabolome data. The phosphoproteome data used in this study was obtained from Fao cells stimulated with single dose (1 nM) of insulin by using non-targeted proteomic measurement [32]. Therefore, it was difficult to calculate the EC_{50} and the $T_{1/2}$ values of phosphorylations of molecules in the trans-omic regulatory network based on the phosphoproteome data, it is based on the western blotting data instead. Targeted-proteomic measurement such as multiple reaction monitoring (MRM) developed recently will provide further information for more comprehensive analysis.

I propose that the methods of reconstruction of a global regulatory trans-omic network and identification of the selectivity of the molecules in the trans-omic regulatory network Comparing sensitivities and time constants of molecules in a trans-omic network with *in vivo* doses and temporal patterns of extracellular stimuli and hormones enable us to estimate selectively of specific pathways and molecules in a trans-omic network depending on doses and temporal patterns of extracellular cytokines or hormones.

5. Experimental Procedures

Identification of differentially phosphorylated proteins

The phosphoproteome data acquired in time series (0, 2, 5, 15, 30, 45, and 60 min) after stimulation with 1 nM insulin [32], was obtained from JPOST (S0000000476). Since the phosphoproteome data consists of two time series of datasets (0, 5, 10, and 45 min and 2, 10, 30, and 60 min), some of the phosphopeptides were identified and quantified in only a time series of a dataset. Therefore a fold change of phosphorylation intensity was calculated as a ratio of the phosphorylation intensity at each time point to the phosphorylation intensity at t = 0 or 2 min. A phosphopeptide exhibiting phosphorylation intensity greater than 1.5-fold increase or less than a 0.67-fold decrease at one or more time points by insulin stimulation was determined as an IRpP. A proteins including at least one IRpP was defined as a differentially phosphorylated proteins.

Identification of signaling layer

The pathways including the character string of “signaling pathway” in their names were extracted from the KEGG database [82,83]. These pathways are defined as signaling pathways in this study. Over-representation of the differentially phosphorylated proteins in

the signaling pathways were determined by using Fisher's exact test [84] with FDR using Storey's procedure [85], and identified the signaling pathways indicating significant over-representation ($FDR < 0.1$). Since the molecules included in the signaling pathways are not mutually exclusive, I integrated these signaling pathways in which the differentially phosphorylated proteins were significantly over-represented into a single network. The molecules, expression of mRNA of which were determined not to express based on the transcriptome data from rat hepatoma Fao cells [38], and those not locating in the downstream of InsR were removed from the network.

Identification of cellular functional pathways responsive to insulin stimulation

I extracted the rat pathways from KEGG database except for the defined signaling pathways (43 pathways), the global pathways (rno01XXX) including Metabolic pathways (rno01100) (9 pathways), the disease related pathways (rno05XXX) (63 pathways), the pathways that work in specific tissues other than liver (52 pathways) (Table S2), and the pathways including the character string of "diabetes", "NAFLD", or "Insulin resistance" in their names (8 pathways). These pathways are defined as cellular functional pathways in this study. The global pathways and disease-related pathways were excluded from the

cellular functional pathways because of redundancy with other cellular functional pathways as subsets. The pathways that work in specific tissues other than liver were excluded from the cellular functional pathways because the Fao cells used in this study were established from rat hepatoma. Over-representation of the differentially phosphorylated proteins in the cellular functional pathways were determined by using Fisher's exact test [84] with FDR using Storey's procedure [85], and identified the cellular functional pathways indicating significant over-representation ($FDR < 0.1$). Among the cellular functional pathways, those in which the differentially phosphorylated proteins were significantly over-represented were defined as a cellular functional layer.

Estimation of RPKs

The KSRs for the amino acid sequences of the proteins including the IRpPs were estimated by using NetPhorest (http://netphorest.info/download/netphorest_human.tsv.xz) [63,64]. Amino acid sequences of rat protein associated with IPI [86] in FASTA format (ftp://ftp.ebi.ac.uk/pub/databases/IPI/current/ipi.RAT.fasta.gz) were used as the inputs for NetPhorest. NetPhorest outputs posterior probabilities that a particular protein kinase classifier recognizes an amino acid residue. Among the candidate classifiers, a classifier

indicating the largest posterior probability value was identified as the kinase classifier recognizing the amino acid sequence. Kinases in each classifier were identified from the website of NetPhorest (view-source:http://netphorest.info/download.shtml) (Table S3), and those included in the classifier indicating the largest posterior probability value were identified as RPKs.

Calculating the Occurrence Rates of RPKs in each pathways

The occurrence rate of a specific kinase classifier (*i*) in a specific pathway (*j*) was calculated as the ratio of the number of IRpPs estimated as a target of the kinase classifier *i* to the number of those included in the pathways *j*. The sum of occurrence rates of the kinase classifiers in pathway *j* is 1.

Clustering the Cellular functional Pathways and Metabolic Enzymes

The pathways included in the cellular functional layer and the metabolic enzymes were hierarchically clustered by using the occurrence rate of the estimated RPKs. The hierarchical clustering was performed using the Euclidean distance for calculation of the intracluster distances and using Ward's method [87] for calculation of the intercluster distances.

Generation of motif logos

The amino acid sequences provided as from -5 to +5 residues from the phosphorylated residues in the IRpPs included in each pathways in the cellular functional layer were extracted. Similarly, the amino acid sequences in the IRpPs included in the metabolic enzymes identified from KEGG database were also extracted. Motif logos of the amino acid sequences in each pathways and the metabolic enzymes were generated using enoLOGOS (http://biodev.hgen.pitt.edu/enologos/) [65] with relative entropy as logo plot methods. Statistical tests of amino acid compositions at each position in the amino acid sequences in each pathways and the metabolic enzymes were performed using iceLogo (http://iomics.ugent.be/icelogoserver/index.html) [66] with percentage difference as scoring system and p value cut-off of 0.05. The Rattus norvegicus amino acid compositions from Swiss-Prot and IRpPs included in cellular functions and metabolic enzymes were used as references compositions for the statistic tests of cellular functional pathways and metabolic enzymes, and each cluster, respectively.

Identification of up-regulated and down-regulated DEGs

The transcriptome data acquired in time series (0, 15, 30, 60, 90, 120, and 240 min) after stimulation with multiple dose of insulin (0.01, 1, 100 nM) [38], was obtained from DDBJ (DRA004341). In the previous study, Sano *et al*. aligned each sequence read to the rat Rnor_5.0 genome using TopHat2 version 2.0.7 [88,89]. Read counts for the genes were annotated in rat Rnor_5.0, and the differentially expressed transcripts were determined using Cuffdiff [38,88,90]. Among all genes corresponding to the differentially expressed transcripts, the genes whose fragments per kilobase of transcript per million mapped reads (FPKM) were obtained at all time points were defined as the DEGs in this study.

The fold changes of FPKMs against those at 0 min were calculated for each DEG. The logarithms of fold changes (log_2FC) were calculated to make the range of up-regulation and down-regulation comparable. The log_2FC were normalized between 0 and 1 to exclude the influence of constitutive expression. *Pt* value were defined as an index of expression variation; sum of absolute values of differences between the slopes between at specific time points and at earlier or later time points, in response to 0.01 nM and 100 nM insulin stimulation (Fig. 5a). The smaller *Pt* value indicates that the time series of gene expression is smoother. *AUC_ratio* was defined as an index of response; the ratio of AUC in response

to 100 nM and that in response to 0.01 nM insulin (Fig. 5a). The larger the absolute value of *AUC_ratio* indicates that the response to insulin is larger. Here, DEGs whose *Pt* value was larger than 0.2 were excluded because of low quality of quantification. Among the DEGs whose *Pt* values were less than 0.2, those with the *AUC_ratio*s of more than $2^{0.5}$ were defined as up-regulated DEGs, and those with the *AUC_ratio*s of less than $2^{-0.5}$ were defined as down-regulated DEGs.

Estimation of sensitivities (EC_{50}) and time constant ($T_{1/2}$)

EC_{50} was defined as the dose of insulin that gives the 50% of the maximal AUC of the time series of log_2FC (Fig. 5c). Since the time when the response reaches the peak in response to insulin are different for individual molecules, the EC_{50} values were calculated based on AUC. $T_{1/2}$ was defined as the time when the response reached 50% of the peak amplitude in the time series of log_2FC against 100 nM insulin stimulation (Fig. 5c). The distributions of EC_{50} and $T_{1/2}$ between the up-regulated and down-regulated DEGs, or between the increased and decreased DCMs were compared using Wilcoxon rank sum test [91,92] with multiple correction using Bonferroni correction [93].

Classification of the molecules in the trans-omic regulatory network

To characterize the molecules in the trans-omic regulatory network by the calculated sensitivities and time constants in response to insulin stimulation, those were classified by using the EC_{50} and the $T_{1/2}$ values. The thresholds dividing the EC_{50} values into high or low sensitivity in, and the $T_{1/2}$ values into fast or slow responses, were determined using Otsu method [94]. The thresholds in the DEGs and the DCMs were determined based on the transcriptome and the metabolome data, respectively, and those in the signaling molecules were determined based on the western blotting data. The signaling molecules, the DEGs, and the DCMs were classified into four classes according to the thresholds (θ_1 for EC_{50}, and θ_2 for $T_{1/2}$): Class 1, high sensitivity ($EC_{50} < \theta_1$) and fast response ($T_{1/2} < \theta_2$) and; Class 2, high sensitivity and slow response ($T_{1/2} > \theta_2$); Class 3, low sensitivity ($EC_{50} > \theta_1$) and fast response, and Class 4, low sensitivity and slow response.

Estimation of TFs regulating each class of DEGs

The flanking regions around the major TSS of each DEG were identified from Rnor_5.0 (Ensembl, release 73) obtained from Ensembl BioMart [95]. The genomic region from -300 bp to +100 bp of the major TSSs were considered as the flanking regions, according to the

FANTOM5 time course analysis [96]. Using TRNASFAC Pro [67], that is a TF database, and Match [68], that is a TFBMs estimation tool, the TFBMs that can bind to each flanking region were estimated. The extended *vertebrate_non_redundant_min_SUM.prf*, one of the parameter set prepared in TRANSFAC Pro, was used for the threshold of similarity score calculated by Match. Since some of the TFs known to be regulated by insulin including FOXO1 are not included in this parameter set, the TFBMs not included in *vertebrate_non_redundant_min_SUM.prf* and related to TFs included in KEGG *insulin signaling pathway* (rno4910), were extracted from *vertebrate_non_redundant.prf*, and appended these TFBMs and their parameters to *vertebrate_non_redundant_min_SUM.prf*. The binding sites within each flanking region were estimated using Match with the extended *vertebrate_non_redundant_min_SUM.prf*. With the estimated TFBMs for each flanking regions related to the DEGs, the TFs regulating the DEGs included in each class were determined. The enrichment of TFBM binding sites in the flanking regions of DEGs in each class were determined using Fisher's exact test [84] with FDR using Storey's procedure [85]. The TFs related to significantly enriched TFBMs ($FDR < 0.1$) were identified as the TFs regulating DEGs included in each class. The TFs related to significantly enriched TFBMs were identified as the TFs regulating DEGs in each class.

Identification of regulators of TFs

IDs of TFBMs and TFs are provided in accession numbers defined within TRANSFAC database. The accession numbers of significantly enriched TFBMs were associated with those of TFs using the correspondence obtained from *matrix.dat* in TRANSFAC Pro. The accession numbers of TFs provided in TRANSFAC Pro are associated with the gene IDs of DATF, EMBL, FLYBASE, MIRBASE, PATHODB, PDB, SMARTDB, SWISSPROT, TRANSCOMPEL, or TRANSPATH. To identify regulators of the TFs, the gene IDs of EMBL, PDB, or SWISSPROT associated with the accession numbers of human, mouse, and rat TF were converted to KEGG gene IDs using bioDBnet (https://biodbnet-abcc.ncifcrf.gov/) [97]. The upstream molecules of the TFs were obtained from the pathway information of KEGG manually, and except for those in the diseases related pathways (rno05XXX) were defined as regulators (Table S8).

Sample preparation for metabolome and western blotting analysis

Rat hepatoma FAO cells were seeded at a density of 3×10^6 cells per dish on 6-cm dishes (Corning) or 1.3×10^6 cells per well on six-well plates (Iwaki) and cultured in RPMI 1640 supplemented with 10% (v/v) fetal bovine serum at 37ºC under 5% CO_2 for 2 days before

deprivation of serum (starvation). The cells were washed twice with phosphate-buffered saline (PBS) and starved in serum-free medium including 0.01 nM insulin (Sigma-Aldrich) and 10 nM dexamethasone (Wako), which increases the expression of gluconeogenesis genes such as *G6pase* and *Pck1* for 16 hours [98]. Hatano continuously added 0.01 nM insulin before the stimulation, and 0.01 nM insulin was present throughout the experiments unless otherwise specified to mimic the *in vivo* constitutive secretion during fasting [57]. The medium was changed at 4 and 2 hours before the stimulation. Cells were stimulated with the indicated doses of insulin by adding 100-fold concentrated stock of insulin solution.

Metabolome analysis

For metabolomics analyses, the cells were washed with 4 mL ice-cold 5% mannitol twice and extracted metabolites with 1 mL of ice-cold methanol including reference compounds (25 μM L-methionine sulfone (Wako), 2-Morpholinoethanesulfonic acid, monohydrate (Dojindo), and D-Camphor-10-sulfonic acid (Wako)) for normalization of peak intensities of mass spectrometry among samples at the indicated times after insulin stimulation. 400 μL of resulting supernatant was sequentially mixed with 200 μL of water and 400 μL of

chloroform, and then centrifuged at 12,000 × *g* for 15 min at 4ºC. The separated aqueous layer was filtered through a 5 kDa cutoff filter (Millipore) to remove proteins. 320 μL of the filtrate was lyophilized and dissolved in 50 μL water including reference compounds (200 μM each of trimesate (Wako) and 3-aminopyrrolidine (Sigma-Aldrich)) for migration time and then injected into the capillary electrophoresis time-of-flight mass spectrometry (CE-TOFMS) system (Agilent Technologies) [49,99,100].

Identification of DCMs

DCMs were identified based on three-way analysis of variance (ANOVA) by comparing three factors: temporal changes of metabolites against the value at 0 min; dose responses in response to 0.01 and 100 nM insulin stimulation at each time points; and the data set measured in different days (n=3). To make the ranges of increase and decrease of the DCMs comparable, log_2FC of abundance of metabolites against the mean abundance at 0 min was calculated for each metabolite. The three-way ANOVA was performed with insulin doses (0.01 and 100 nM), time points after insulin stimulation (0, 5, 15, 30, 60, 90, 120, and 240 min), and data sets using the logarithmic values of fold changes. The p values against insulin doses were calculated and FDR of each metabolite were calculated by using

Storey's procedures [85]. The λ value to calculate FDR was set to 0.8 with reference to the distribution of *p* values. The metabolites showing significance (*FDR* < 0.1) were defined as DCMs.

Definition of increased and decreased DCMs

Increased and decreased DCMs were defined using the same procedure as identification of the up-regulated and down-regulated DEGs. For each DCM, the fold change of abundance of metabolites at each time point to the mean abundance at 0 min was calculated. To make the ranges of increase and decrease of the DCMs comparable, log_2FCs of abundance of metabolites against the mean abundance at 0 min was calculated for each metabolite, and normalized between 0 and 1. The *AUC_ratio*s, which is the ratio of AUC with 100 nM insulin to AUC with 0.01 nM stimulation, were calculated based on the log_2FCs. The metabolites with the *AUC_ratio*s of more than $2^{0.5}$ were defined as increased, and those with the *AUC_ratio*s of less than $2^{-0.5}$ were defined as decreased DCMs.

Identification of RMEs

The enzymatic reactions involved to the identified DCMs were comprehensively searched based on the data downloaded from the KEGG database. The DCMs except hub

metabolites, determined according to previous studies of network topology [101], were regarded as targets of RMEs. All of the enzymes with substrates or products that include at least one DCM except the hub metabolites were identified, and defined as RMEs.

Identification of allosteric regulation

The entries for the RMEs related to allosteric regulation were obtained from the BRENDA database (http://www.brenda-enzymes.org) [71], a literature-based database providing information regarding allosteric effectors and their target enzymes from. Allosteric effector (activator and inhibitor) of the RMEs provided in BRENDA database were identified, as reported for mammals (*Bos Taurus*, *Felis catus*, *Homo sapiens*, "Macaca", "Mammalia", "Monkey", *Mus booduga*, *Mus musculus*, *Rattus norvegicus*, *Rattus rattus*, *Rattus* sp., *Sus scrofa*, "dolphin", and "hamster"). The standard compound names of allosteric effectors used in BRENDA were associated with metabolite names that were used in KEGG to obtain the KEGG compound ID related to each allosteric effector. Finally, the allosteric effectors, related to the RMEs, included in the DCMs were extracted.

Western blotting

For western blotting, the same insulin-stimulated cells as those used for metabolome analysis were washed with ice-cold PBS and extracted proteins with 50 mM Tris-Cl pH 8.8 including 1% SDS at the indicated times after insulin stimulation. The lysates were sonicated and centrifuged at 12,000 × *g* at 4 ºC for 15 min to remove debris. The resulting supernatants were subjected to measurement by western blotting. The antibodies used for the western blotting analysis were represented in Table 5.

6. Figures

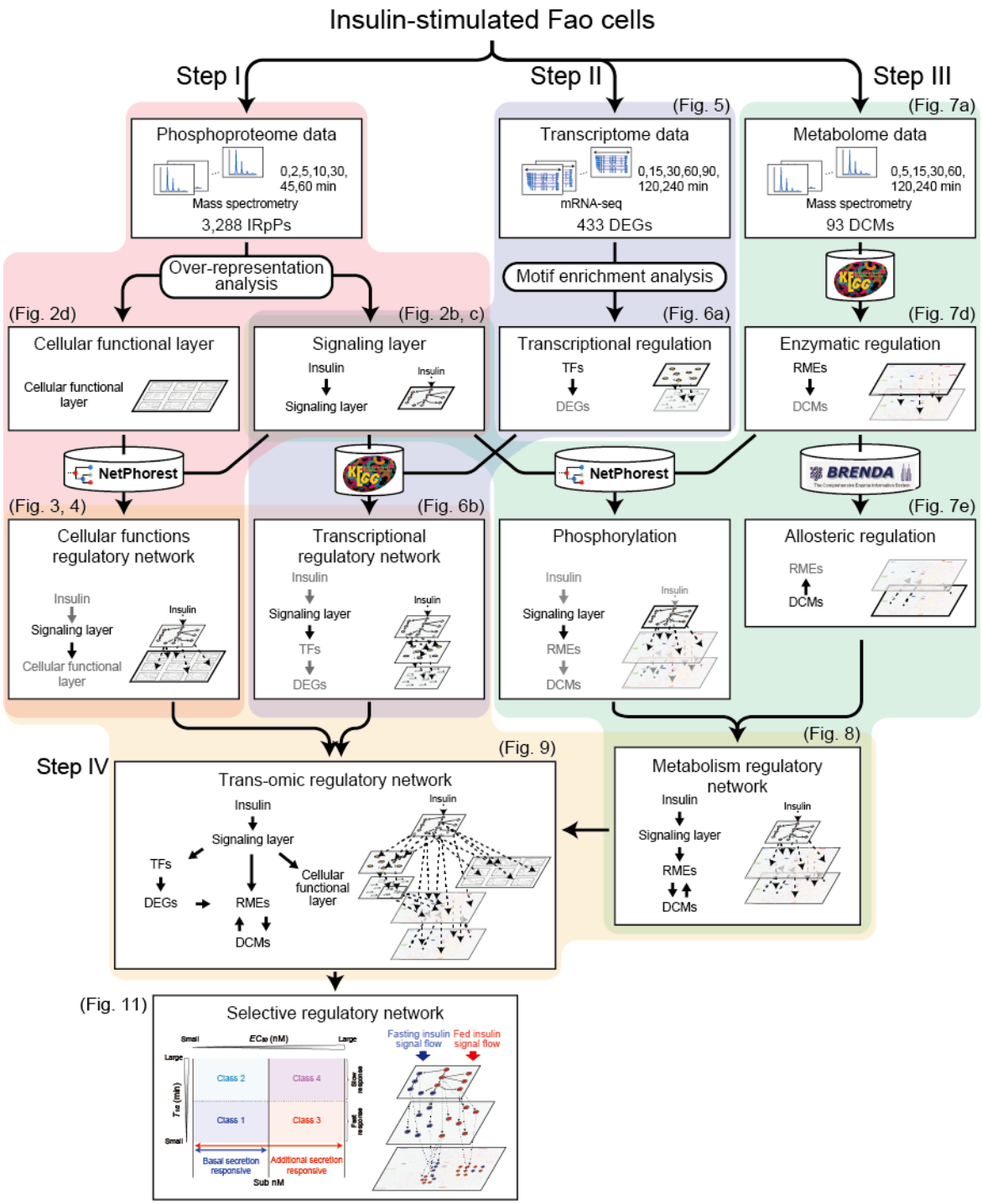
Insulin-stimulated Fao cells
Step I
Step II
Step III
Phosphoproteome data
0,2,5,10,30, 45,60 min
Mass spectrometry
3,288 IRpPs
Transcriptome data
0,15,30,60,90, 120,240 min
mRNA-seq
433 DEGs
(Fig. 5)
Metabolome data
0,5,15,30,60, 120,240 min
Mass spectrometry
93 DCMs
(Fig. 7a)
Over-representation analysis
Motif enrichment analysis
(Fig. 2d)
(Fig. 2b, c)
(Fig. 6a)
(Fig. 7d)
Cellular functional layer
Signaling layer
Transcriptional regulation
Enzymatic regulation
TFs
DEGs
RMEs
DCMs
NetPhorest
NetPhorest
BRENDA
(Fig. 3, 4)
(Fig. 6b)
(Fig. 7e)
Cellular functions regulatory network
Transcriptional regulatory network
Phosphorylation
Allosteric regulation
Step IV
(Fig. 9)
(Fig. 8)
Trans-omic regulatory network
Metabolism regulatory network
(Fig. 11)
Selective regulatory network
Fasting insulin signal flow
Fed insulin signal flow
Class 1
Class 2
Class 3
Class 4
Basal secretion responsive
Additional secretion responsive

Fig. 1 | Summary of reconstruction of trans-omic regulatory network.

The trans-omic regulatory network was reconstructed by integrating the networks based on phosphoproteome, transcriptome, and metabolome data consisting of the Steps I to VI. Selectivity of the molecules in the trans-omic regulatory network were estimated according to their EC_{50} and $T_{1/2}$ values calculated based on the western blotting, transcriptome, and metabolome data.

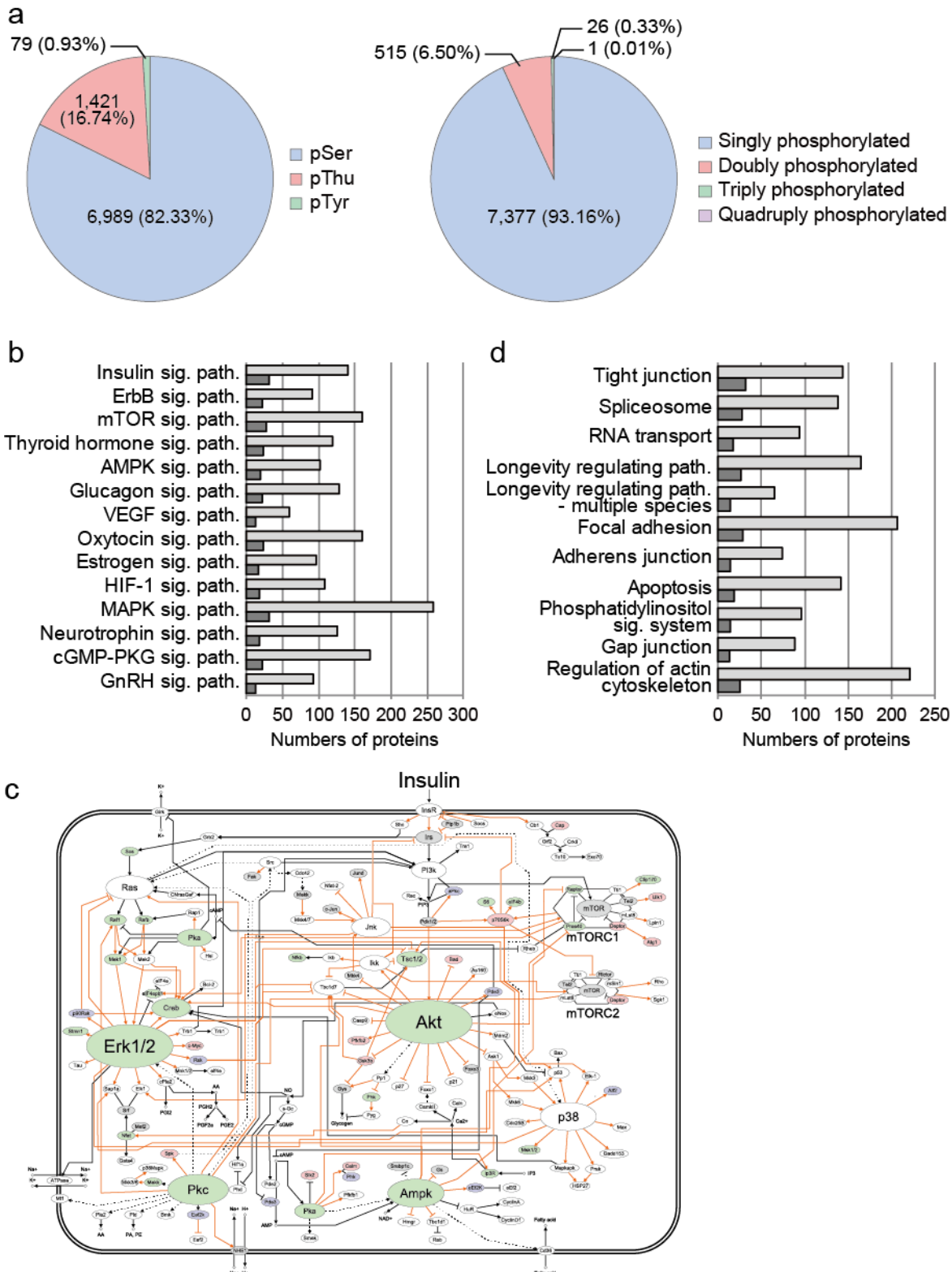
a
79 (0.93%)
1,421 (16.74%)
6,989 (82.33%)
pSer
pThu
pTyr
515 (6.50%)
26 (0.33%)
1 (0.01%)
7,377 (93.16%)
Singly phosphorylated
Doubly phosphorylated
Triply phosphorylated
Quadruply phosphorylated
b
Insulin sig. path.
ErbB sig. path.
mTOR sig. path.
Thyroid hormone sig. path.
AMPK sig. path.
Glucagon sig. path.
VEGF sig. path.
Oxytocin sig. path.
Estrogen sig. path.
HIF-1 sig. path.
MAPK sig. path.
Neurotrophin sig. path.
cGMP-PKG sig. path.
GnRH sig. path.
0 50 100 150 200 250 300
Numbers of proteins
d
Tight junction
Spliceosome
RNA transport
Longevity regulating path.
Longevity regulating path. - multiple species
Focal adhesion
Adherens junction
Apoptosis
Phosphatidylinositol sig. system
Gap junction
Regulation of actin cytoskeleton
0 50 100 150 200 250
Numbers of proteins
c
Insulin
Rtks
PI3k
Ras
Jnk
mTOR
mTORC1
mTORC2
Ikk
Tsc1/2
Akt
Creb
Erk1/2
p38
Pkc
Ampk

Fig. 2 | Identification of signaling layer.

(a) Distribution of detected phosphorylated amino acid residues in the phosphoproteome data, and that of numbers of phosphorylated sites per peptide. Numbers and parentheses indicate the number of amino acid residues or phosphopeptides and percentage relative to the total amino acid residues or phosphopeptides, respectively. (b) Numbers of differentially phosphorylated proteins in the signaling pathways. The light gray and dark gray bars indicate the total numbers of proteins and differentially phosphorylated proteins included in each signaling pathway, respectively. (c) Identified signaling layer. Red, blue and green nodes indicate proteins with all of the significantly changed phosphorylated sites exhibiting an increase (> 1.5-fold) or a decrease (< 0.67-fold) or both, respectively. Gray and white nodes indicate proteins with unchanged phosphorylation and with no phosphorylation detected, respectively. Size of a node indicates number of its interactions with other molecules. Orange edges indicate phosphorylation. (d) Numbers of differentially phosphorylated proteins in the cellular functional pathways. The light gray and dark gray bars indicate the total numbers of proteins and differentially phosphorylated proteins included in each cellular functional pathway, respectively.

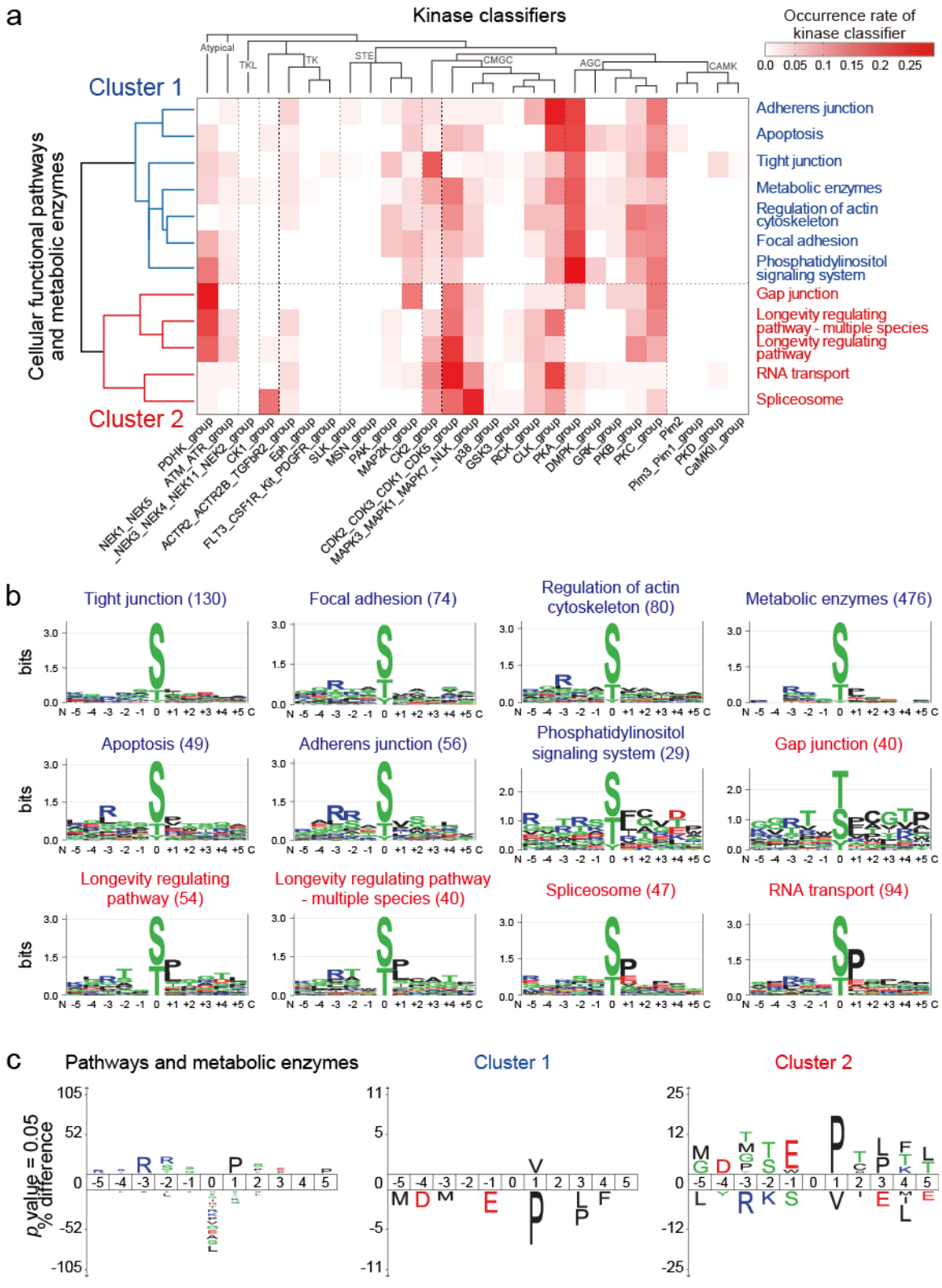
a
Kinase classifiers
Occurrence rate of kinase classifier
0.0 0.05 0.1 0.15 0.2 0.25
Atypical
TKL
TK
STE
CMGC
AGC
CAMK
Cluster 1
Cluster 2
Cellular functional pathways and metabolic enzymes
Adherens junction
Apoptosis
Tight junction
Metabolic enzymes
Regulation of actin cytoskeleton
Focal adhesion
Phosphatidylinositol signaling system
Gap junction
Longevity regulating pathway - multiple species
Longevity regulating pathway
RNA transport
Spliceosome
PDHK_group
ATM_ATR_group
CK1_group
Eph_group
SLK_group
MSN_group
PAK_group
MAP2K_group
CK2_group
p38_group
GSK3_group
RCK_group
CLK_group
PKA_group
DMPK_group
GRK_group
PKB_group
PKC_group
Pim2
Pim3_Pim1_group
PKD_group
CaMKII_group
NEK1_NEK5_NEK3_NEK4_NEK11_NEK2_group
ACTR2_ACTR2B_TGFbR2_group
FLT3_CSF1R_Kit_PDGFR_group
CDK2_CDK3_CDK1_CDK5_group
MAPK3_MAPK1_MAPK7_NLK_group
b
Tight junction (130)
Focal adhesion (74)
Regulation of actin cytoskeleton (80)
Metabolic enzymes (476)
Apoptosis (49)
Adherens junction (56)
Phosphatidylinositol signaling system (29)
Gap junction (40)
Longevity regulating pathway (54)
Longevity regulating pathway - multiple species (40)
Spliceosome (47)
RNA transport (94)
bits
N -5 -4 -3 -2 -1 0 +1 +2 +3 +4 +5 C
c
Pathways and metabolic enzymes
Cluster 1
Cluster 2
p value = 0.05
% difference

Fig. 3 | Estimation of KSRs for the IRpPs in cellular functional layer.

(a) Clustering analysis of cellular functional pathways and metabolic enzymes. The pathways and metabolic enzymes were hierarchically clustered by the calculated occurrence ratios against the kinase classifier. The deeper red indicates higher occurrence ratio. (b) Amino acid motifs logo indicating frequency of the amino acid residues at each position. The logos were generated for the amino acid sequences of IRpPs in each pathways and metabolic enzymes. The height of each letter at each position is scaled relative to the information content, reflecting the frequency of the corresponding amino acid. Blue and red pathway names correspond to those in cluster 1 and 2, respectively. The number in parentheses attached to each pathway name represents the number of IRpPs included in the pathway. (c) Amino acid motifs logo indicating statistical representation of the amino acid residues at each position. The logos were generated for the IRpPs included in cellular functional layer and metabolic enzymes (left), cluster 1 (middle), and cluster 2 (right). The characters above and below each horizontal line indicate amino acids showing significant over-representations and under-representations ($p < 0.05$), respectively. The height of the letter representing an amino acid at each position reflects the difference in the frequency of its occurrence in the sets of reference and phosphopeptides.

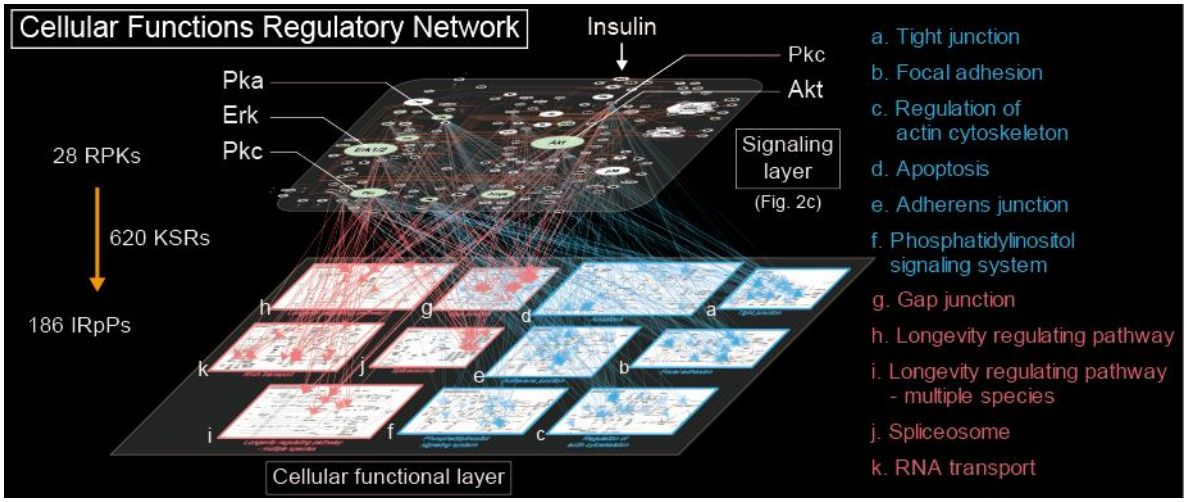
Cellular Functions Regulatory Network
Insulin
Pka
Erk
Pkc
Pkc
Akt
28 RPKs
620 KSRs
186 IRpPs
Signaling layer
(Fig. 2c)
Cellular functional layer
a. Tight junction
b. Focal adhesion
c. Regulation of actin cytoskeleton
d. Apoptosis
e. Adherens junction
f. Phosphatidylinositol signaling system
g. Gap junction
h. Longevity regulating pathway
i. Longevity regulating pathway - multiple species
j. Spliceosome
k. RNA transport

Fig. 4 | Reconstructed cellular functional regulatory network.

The Cellular functions regulatory network was reconstructed based on the phosphoproteome data. The arrows (from the top to the bottom layer) indicate phosphorylations of the IRpPs by the RPKs. The colors of the pathway frames and pathways names correspond to the cluster defined in Fig. 3a.

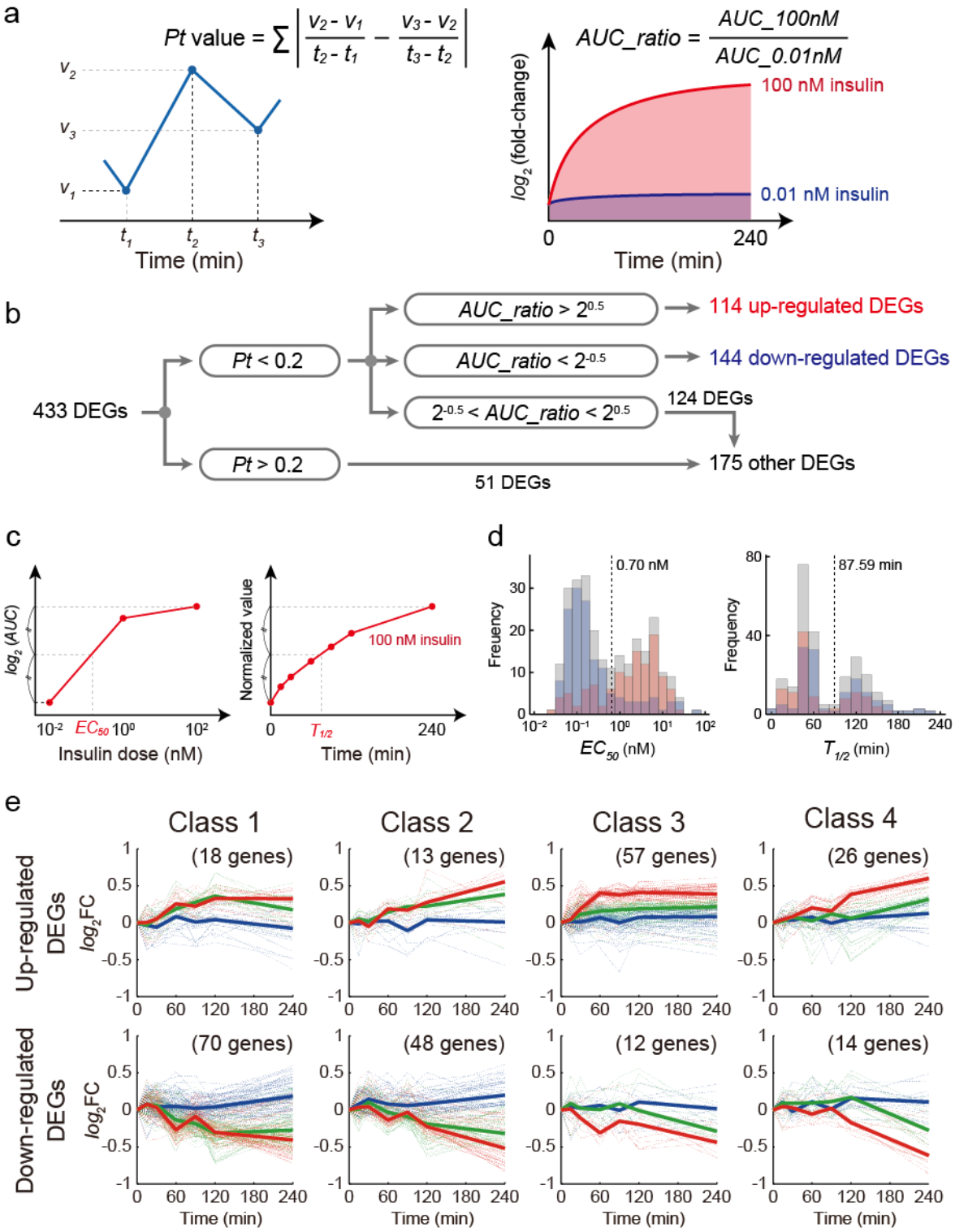
a
Pt value = ∑ | (v2 - v1)/(t2 - t1) − (v3 - v2)/(t3 - t2) |
v2
v3
v1
t1
t2
t3
Time (min)
AUC_ratio = AUC_100nM / AUC_0.01nM
100 nM insulin
0.01 nM insulin
log2 (fold-change)
0
240
Time (min)
b
433 DEGs
Pt < 0.2
Pt > 0.2
AUC_ratio > 2^0.5
AUC_ratio < 2^-0.5
2^-0.5 < AUC_ratio < 2^0.5
114 up-regulated DEGs
144 down-regulated DEGs
124 DEGs
175 other DEGs
51 DEGs
c
log2 (AUC)
10-2
EC50
100
102
Insulin dose (nM)
Normalized value
100 nM insulin
0
T1/2
240
Time (min)
d
Freuency
0.70 nM
EC50 (nM)
Frequency
87.59 min
T1/2 (min)
e
Class 1
Class 2
Class 3
Class 4
Up-regulated DEGs
Down-regulated DEGs
log2FC
(18 genes)
(13 genes)
(57 genes)
(26 genes)
(70 genes)
(48 genes)
(12 genes)
(14 genes)
Time (min)

Fig. 5 | Classification of the DEGs.

(a) Definition of *Pt* value (left) and *AUC_ratio* (right), as indices of expression variation and response, respectively. (b) Definition of the up-regulated and down-regulated DEGs. (c) Definition of EC_{50} (left) and $T_{1/2}$ (right), as indices of sensitivity to insulin doses and time constant, respectively. (d) Distribution of EC_{50} (left) and $T_{1/2}$ (right) values calculated for up-regulated (red) and down-regulated DEGs (blue). Gray bars indicate the sum of the frequency of up-regulated and down-regulated DEGs. The dashed lines indicate the thresholds dividing large and small values. (e) Time courses of DEGs in each class. Dashed lines and bold lines indicate the time series of each DEG and centroids of DEGs included in each class, respectively. Blue, green, and red lines indicate responses to 0.01, 1, and 100 nM insulin, respectively.

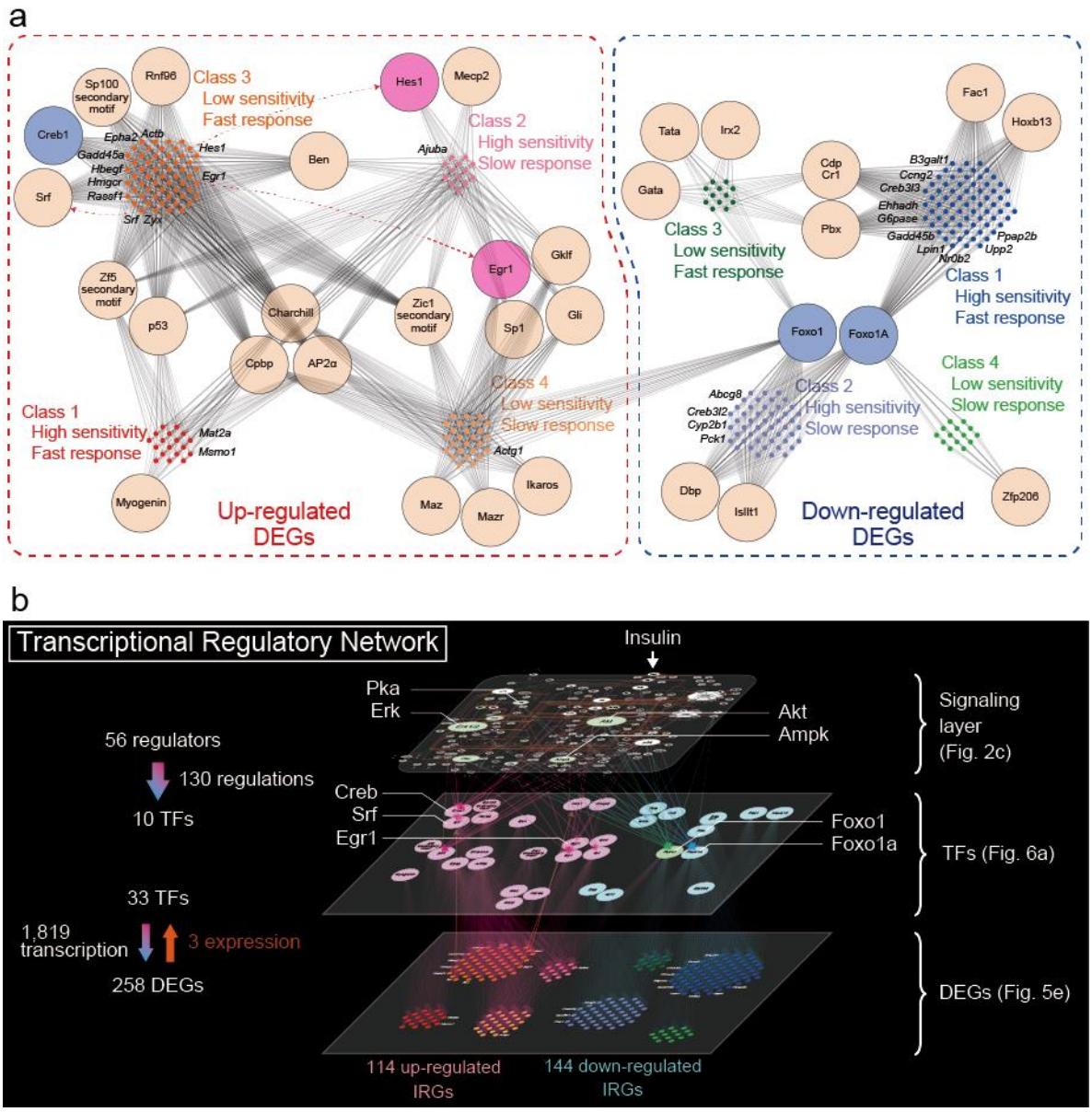
a
Class 3
Low sensitivity
Fast response
Class 2
High sensitivity
Slow response
Class 1
High sensitivity
Fast response
Class 4
Low sensitivity
Slow response
Up-regulated DEGs
Down-regulated DEGs
Rnf96
Sp100 secondary motif
Creb1
Srf
Epha2
Actb
Gadd45a
Hbegf
Hmgcr
Rassf1
Srf
Zyx
Hes1
Egr1
Ben
Hes1
Mecp2
Ajuba
Egr1
Gklf
Gli
Sp1
Zic1 secondary motif
Zf5 secondary motif
p53
Charchill
Cpbp
AP2α
Mat2a
Msmo1
Actg1
Ikaros
Maz
Mazr
Myogenin
Tata
Irx2
Gata
Cdp Cr1
Pbx
Fac1
Hoxb13
B3galt1
Ccng2
Creb3l3
Ehhadh
G6pase
Gadd45b
Lpin1
Nr0b2
Ppap2b
Upp2
Foxo1
Foxo1A
Abcg8
Creb3l2
Cyp2b1
Pck1
Dbp
Islt1
Zfp206

b
Transcriptional Regulatory Network
Insulin
Pka
Erk
Akt
Ampk
Signaling layer (Fig. 2c)
56 regulators
130 regulations
10 TFs
Creb
Srf
Egr1
Foxo1
Foxo1a
TFs (Fig. 6a)
33 TFs
1,819 transcription
3 expression
258 DEGs
DEGs (Fig. 5e)
114 up-regulated IRGs
144 down-regulated IRGs

Fig. 6 | Reconstructed transcriptional regulatory network.

(a) Sets of dots and circles indicate the classes of the DEGs, and the estimated TFs for the classes, respectively. Gray arrows indicate transcriptional regulation by each TF. Red dashed arrows indicate expression of the TF genes included in each DEG class. The colors of the TFs indicate the classes of the TFs classified in Fig. 10b: blue, high sensitivity and fast response (Class 1); magenta, low sensitivity and slow response (Class 4); and pale orange: unmeasured by the western blotting. (b) Reconstructed transcriptional regulatory network. The arrows from the top to the middle layer indicate regulations of the TFs by their regulators. The arrows from the middle to the bottom layer indicate transcription of the DEGs. The arrows from the bottom to the middle layer indicate expression of the TF genes.

.

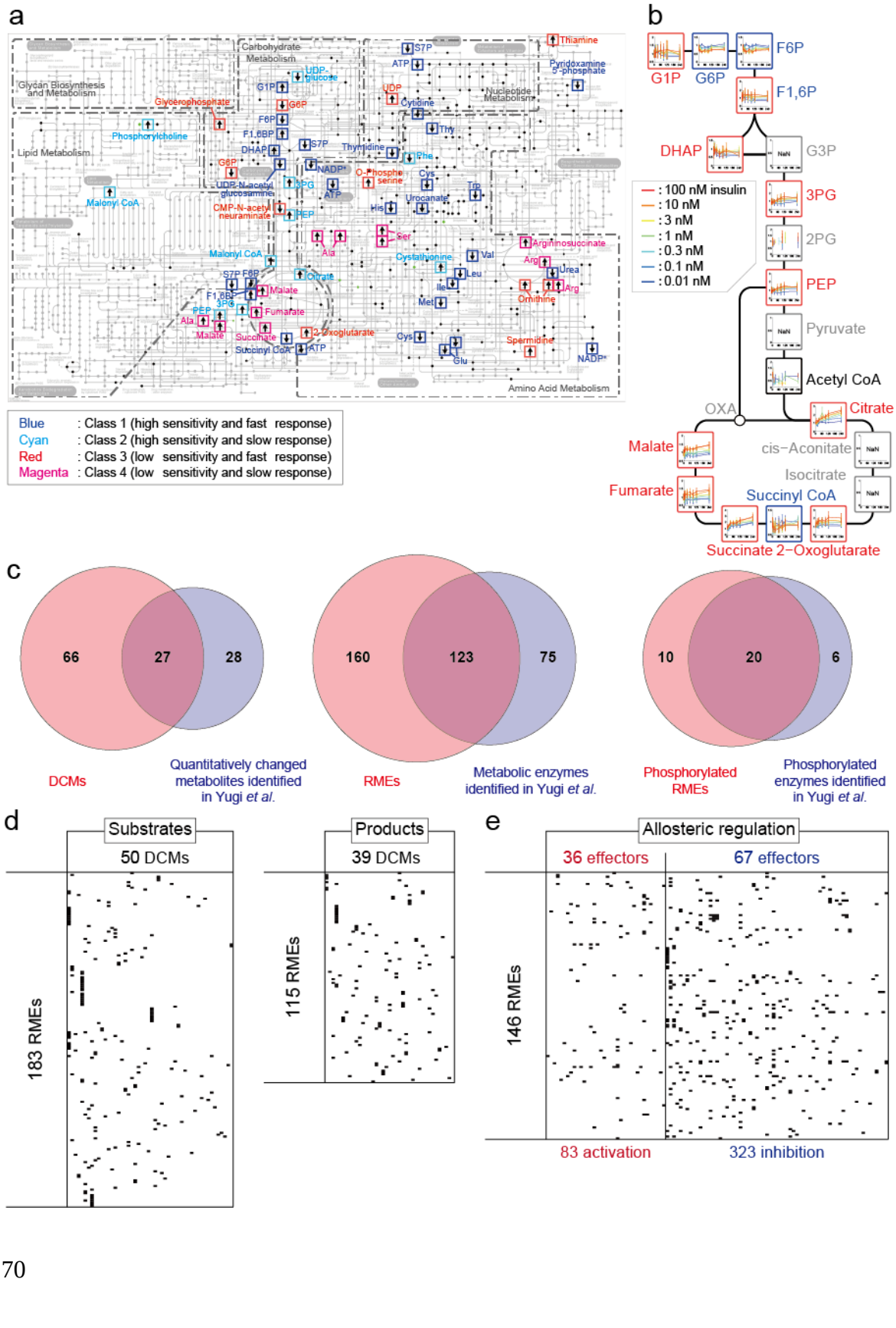
a
Carbohydrate Metabolism
Glycan Biosynthesis and Metabolism
Lipid Metabolism
Nucleotide Metabolism
Amino Acid Metabolism
Blue : Class 1 (high sensitivity and fast response)
Cyan : Class 2 (high sensitivity and slow response)
Red : Class 3 (low sensitivity and fast response)
Magenta : Class 4 (low sensitivity and slow response)
b
F6P
G1P
G6P
F1,6P
DHAP
G3P
3PG
2PG
PEP
Pyruvate
Acetyl CoA
OXA
Citrate
cis−Aconitate
Isocitrate
Malate
Fumarate
Succinyl CoA
Succinate
2−Oxoglutarate
: 100 nM insulin
: 10 nM
: 3 nM
: 1 nM
: 0.3 nM
: 0.1 nM
: 0.01 nM
c
66
27
28
DCMs
Quantitatively changed metabolites identified in Yugi et al.
160
123
75
RMEs
Metabolic enzymes identified in Yugi et al.
10
20
6
Phosphorylated RMEs
Phosphorylated enzymes identified in Yugi et al.
d
Substrates
50 DCMs
183 RMEs
Products
39 DCMs
115 RMEs
e
Allosteric regulation
36 effectors
67 effectors
146 RMEs
83 activation
323 inhibition

Fig. 7 | Classification of the DCMs and identification of RMEs.

(a) DCMs projected on the KEGG *metabolic pathways* (rno01100). Arrows indicate whether an DCM increased or decreased. The colors of the box outlines indicate the classes of the DCMs classified in Fig. 10b: blue, high sensitivity and fast response (Class 1); Cyan, high sensitivity and slow response (Class 2); red, low sensitivity and fast response (Class 3); and magenta, low sensitivity and slow response (Class4). (b) Metabolites in the central carbon metabolism. The colors of the box outlines indicate whether an DCM increased or decreased: red, increased DCMs; blue, decreased DCMs; black, the metabolites that did not show significant change against insulin doses; and gray, the metabolites including unmeasured points at one and more time points (c) Comparison of DCMs, RMEs, and phosphorylated RMEs identified in this study (red) and those in the previous study [32] (blue). (d) Substrates and products of the RMEs. A dot indicates that the DCM (x-axis) is substrate or a product for a RME (y-axis). (D) Allosteric regulation of the RMEs by the DCMs that function as positive (activation) or negative (inhibition) allosteric effectors. A dot indicates that the DCM (x-axis) is an allosteric effector for a RME (y-axis).

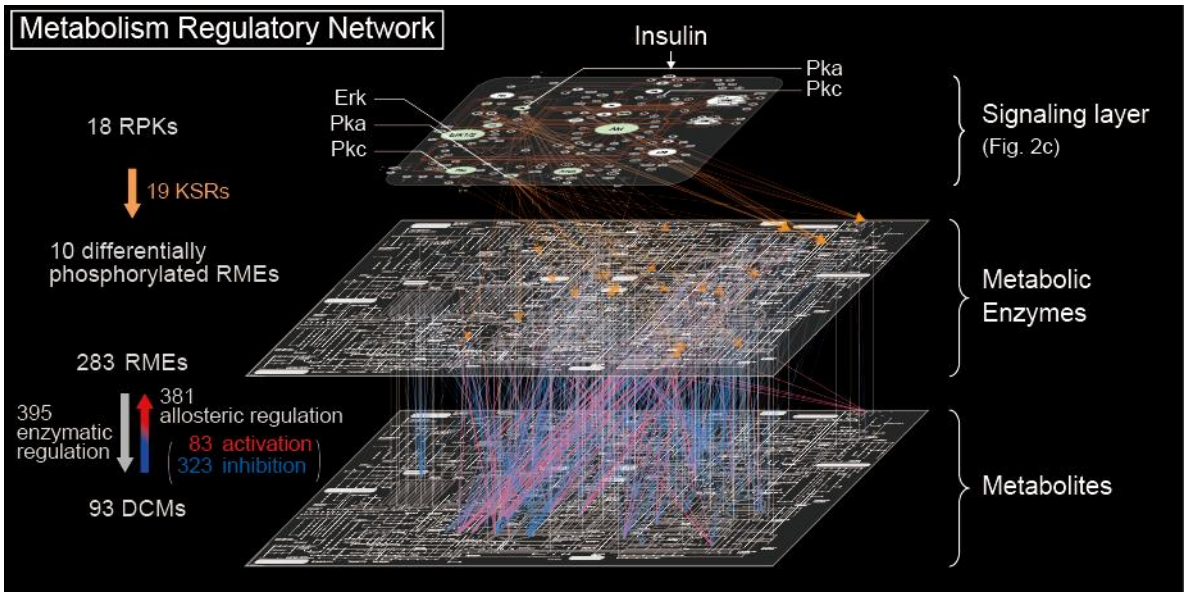
Metabolism Regulatory Network
Insulin
Pka
Pkc
Erk
Pka
Pkc
18 RPKs
19 KSRs
10 differentially phosphorylated RMEs
283 RMEs
395 enzymatic regulation
381 allosteric regulation
83 activation
323 inhibition
93 DCMs
Signaling layer
(Fig. 2c)
Metabolic Enzymes
Metabolites

Fig. 8 | Reconstructed metabolism regulatory network.

Reconstructed metabolism regulatory network. The arrows from the top to the middle layer indicate phosphorylations of the RMEs by their RPKs. The arrows from the middle to the bottom layer indicate enzymatic regulations of the DCMs by their RMEs. The arrows from the bottom to the middle layer indicate allosteric regulation of the RMEs by their allosteric effectors included in DCMs: red, activation; blue, inhibition.

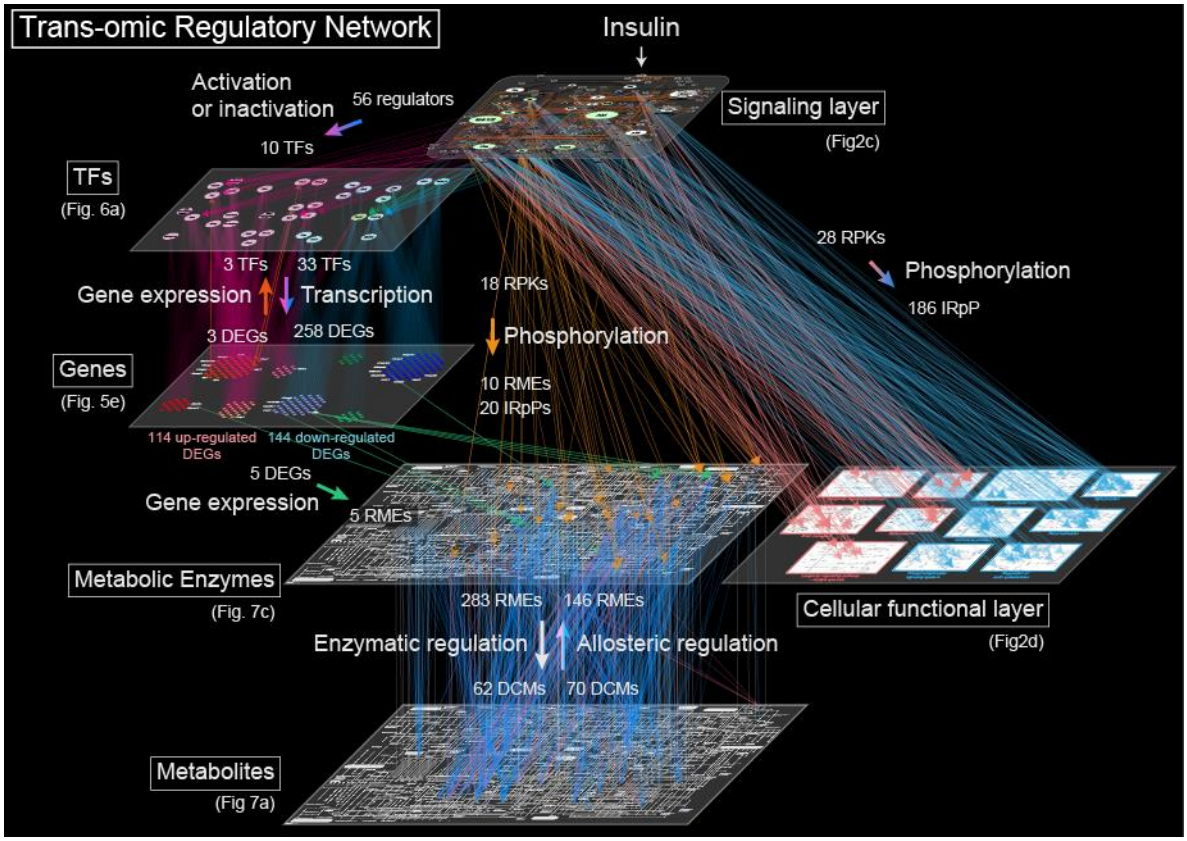
Trans-omic Regulatory Network
Insulin
Activation
or inactivation
56 regulators
10 TFs
Signaling layer
(Fig2c)
TFs
(Fig. 6a)
28 RPKs
Phosphorylation
186 IRpP
3 TFs
33 TFs
Gene expression
Transcription
18 RPKs
3 DEGs
258 DEGs
Phosphorylation
Genes
(Fig. 5e)
10 RMEs
20 IRpPs
114 up-regulated DEGs
144 down-regulated DEGs
5 DEGs
Gene expression
5 RMEs
Metabolic Enzymes
(Fig. 7c)
283 RMEs
146 RMEs
Cellular functional layer
(Fig2d)
Enzymatic regulation
Allosteric regulation
62 DCMs
70 DCMs
Metabolites
(Fig 7a)

Fig. 9 | Reconstruction of trans-omic regulatory network.

Trans-omic regulatory network was reconstructed by integration of the cellular functions regulatory network (Fig. 4, Step I), the transcriptional regulatory network (Fig. 6b, Step II), and the metabolism regulatory network (Fig. 8, Step III).

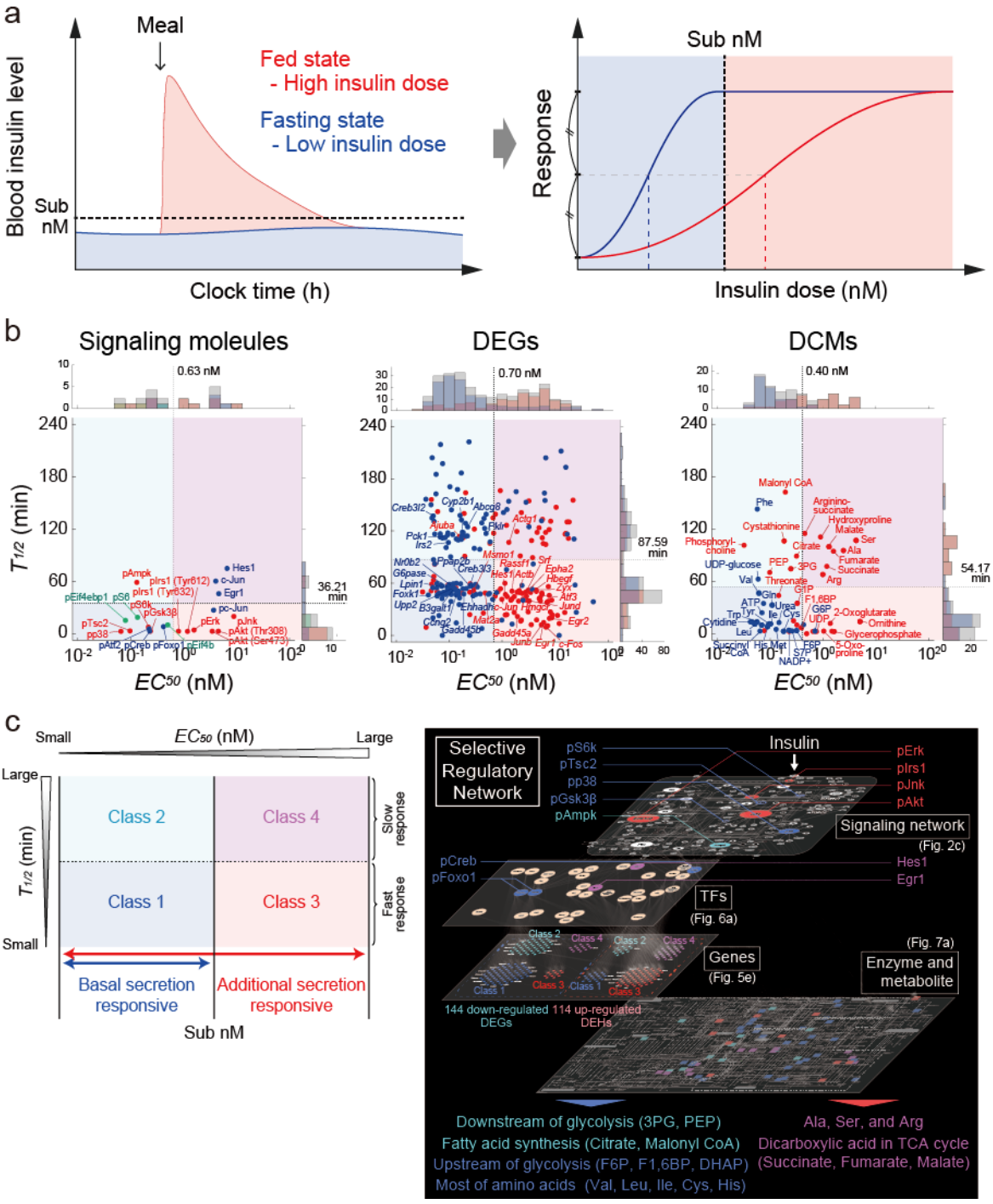
a
Meal
Fed state
- High insulin dose
Fasting state
- Low insulin dose
Blood insulin level
Sub nM
Clock time (h)
Sub nM
Response
Insulin dose (nM)
b
Signaling moleules
DEGs
DCMs
0.63 nM
0.70 nM
0.40 nM
T1/2 (min)
87.59 min
36.21 min
54.17 min
EC50 (nM)
c
Small
EC50 (nM)
Large
Class 2
Class 4
Class 1
Class 3
Slow response
Fast response
Basal secretion responsive
Additional secretion responsive
Sub nM
Selective Regulatory Network
Insulin
pS6k
pTsc2
pp38
pGsk3β
pAmpk
pErk
pIrs1
pJnk
pAkt
Signaling network
(Fig. 2c)
pCreb
pFoxo1
Hes1
Egr1
TFs
(Fig. 6a)
Genes
(Fig. 5e)
(Fig. 7a)
Enzyme and metabolite
144 down-regulated DEGs
114 up-regulated DEHs
Downstream of glycolysis (3PG, PEP)
Fatty acid synthesis (Citrate, Malonyl CoA)
Upstream of glycolysis (F6P, F1,6BP, DHAP)
Most of amino acids (Val, Leu, Ile, Cys, His)
Ala, Ser, and Arg
Dicarboxylic acid in TCA cycle
(Succinate, Fumarate, Malate)

Fig. 10 | Selectivity of the molecules in the trans-omic regulatory network.

(a) Temporal secretion patterns of insulin *in vivo* [57], and scheme of selectivity of each molecule with insulin temporal patterns. The molecules indicating high sensitivities (blue in right panel) mainly response to basal secretion of insulin under sub nM, while those indicating low sensitivities (red in right panel) distinguish basal and additional secretion of insulin. (b) The distributions of the EC_{50} and the $T_{1/2}$ values of the signaling molecules (left), the DEGs (middle), and the DCMs (right). Red, blue, and green dots in the signaling molecules indicate signaling factors, TFs, and protein synthesis related factors, respectively. Red and blue dots in the DEGs indicate up-regulated and down-regulated DEGs, respectively. Red and blue dots in the DCMs indicate increased and decreased DCMs, respectively. The dotted lines indicate the thresholds of EC_{50} and $T_{1/2}$ values dividing large and small. (c) Selectivity of the molecules in each classes, and reconstructed selective regulatory network. The molecules indicating high sensitivity (Class 1 and 2) are responsive to basal secretion of insulin (blue and cyan), and those indicating low sensitivity (Class 3 and 4) are responsive to additional secretion (red and magenta). The selectivity of the measured molecules are reflected in the trans-omic regulatory network reconstructed in Fig. 9 as selective regulatory network.

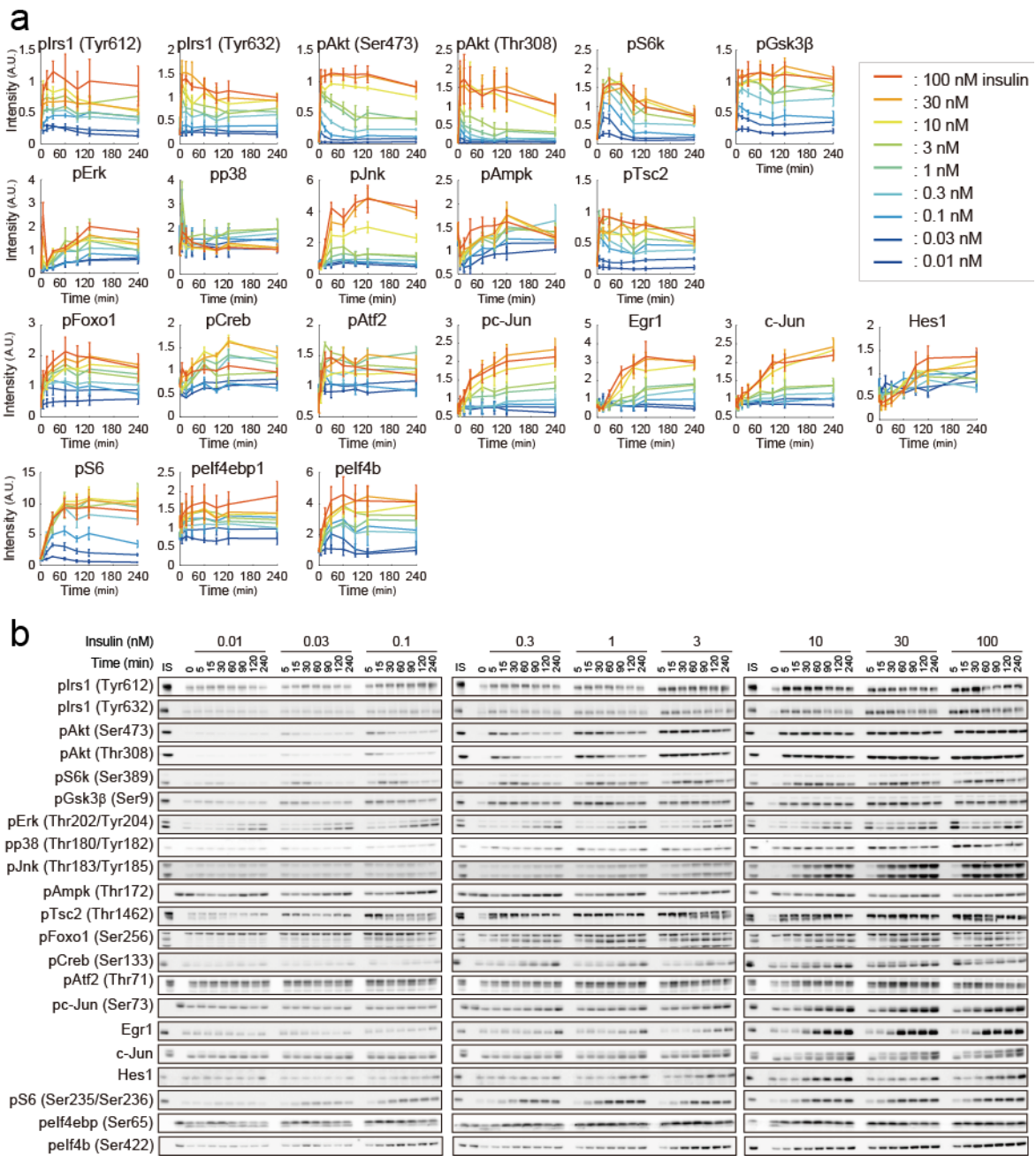
a
pIrs1 (Tyr612)
pIrs1 (Tyr632)
pAkt (Ser473)
pAkt (Thr308)
pS6k
pGsk3β
pErk
pp38
pJnk
pAmpk
pTsc2
pFoxo1
pCreb
pAtf2
pc-Jun
Egr1
c-Jun
Hes1
pS6
pelf4ebp1
pelf4b
Intensity (A.U.)
Time (min)
: 100 nM insulin
: 30 nM
: 10 nM
: 3 nM
: 1 nM
: 0.3 nM
: 0.1 nM
: 0.03 nM
: 0.01 nM
b
Insulin (nM)
Time (min)
IS
pIrs1 (Tyr612)
pIrs1 (Tyr632)
pAkt (Ser473)
pAkt (Thr308)
pS6k (Ser389)
pGsk3β (Ser9)
pErk (Thr202/Tyr204)
pp38 (Thr180/Tyr182)
pJnk (Thr183/Tyr185)
pAmpk (Thr172)
pTsc2 (Thr1462)
pFoxo1 (Ser256)
pCreb (Ser133)
pAtf2 (Thr71)
pc-Jun (Ser73)
Egr1
c-Jun
Hes1
pS6 (Ser235/Ser236)
pelf4ebp (Ser65)
pelf4b (Ser422)

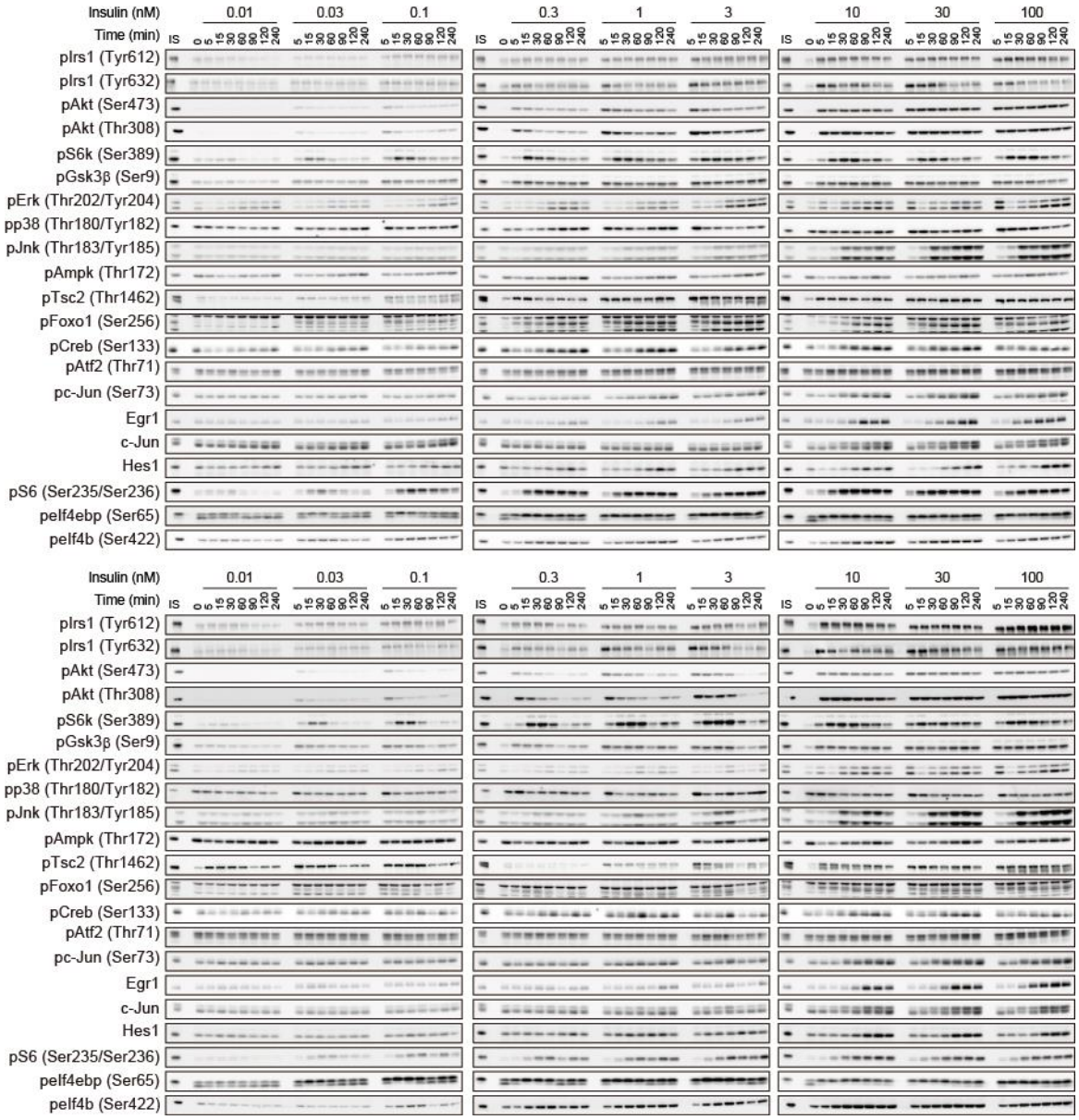
Insulin (nM)
0.01
0.03
0.1
0.3
1
3
10
30
100
Time (min)
IS
0
5
15
30
60
90
120
240
pIrs1 (Tyr612)
pIrs1 (Tyr632)
pAkt (Ser473)
pAkt (Thr308)
pS6k (Ser389)
pGsk3β (Ser9)
pErk (Thr202/Tyr204)
pp38 (Thr180/Tyr182)
pJnk (Thr183/Tyr185)
pAmpk (Thr172)
pTsc2 (Thr1462)
pFoxo1 (Ser256)
pCreb (Ser133)
pAtf2 (Thr71)
pc-Jun (Ser73)
Egr1
c-Jun
Hes1
pS6 (Ser235/Ser236)
pelf4ebp (Ser65)
pelf4b (Ser422)

Fig. 11 | Time courses of the signaling molecules monitored by western blotting.

(a) Time courses of the indicated molecules by the indicated doses of insulin were plotted from data obtained by western blotting. The means and standard error of the means (SEMs) of three independent experiments are shown. Lowercase ‘p’ preceding the name of a protein indicates the detection of the phosphorylated from of the protein. Numbers and letters in parentheses represent the phosphorylated amino acid residue. Numbering according to human. (B) All images of western blotting were shown. IS indicates internal standard.

7. Tables

Table 1 | Signaling pathways in which the differentially phosphorylated proteins were significantly over-represented.

KEGG pathway	Pathway name	Raw *p* value	*FDR*
path:rno04910	Insulin signaling pathway	3.23×10^{-9}	2.41×10^{-7}
path:rno04012	ErbB signaling pathway	1.66×10^{-7}	8.29×10^{-6}
path:rno04150	mTOR signaling pathway	4.08×10^{-6}	1.22×10^{-4}
path:rno04919	Thyroid hormone signaling pathway	6.02×10^{-6}	1.50×10^{-4}
path:rno04922	Glucagon signaling pathway	7.31×10^{-5}	1.16×10^{-3}
path:rno04152	AMPK signaling pathway	7.77×10^{-5}	1.16×10^{-3}
path:rno04370	VEGF signaling pathway	2.30×10^{-4}	2.87×10^{-3}
path:rno04921	Oxytocin signaling pathway	2.94×10^{-4}	3.38×10^{-3}
path:rno04915	Estrogen signaling pathway	3.44×10^{-4}	3.67×10^{-3}
path:rno04066	HIF-1 signaling pathway	5.60×10^{-4}	4.92×10^{-3}
path:rno04010	MAPK signaling pathway	1.05×10^{-3}	8.69×10^{-3}
path:rno04722	Neurotrophin signaling pathway	3.17×10^{-3}	2.49×10^{-2}
path:rno04022	cGMP-PKG signaling pathway	4.30×10^{-3}	3.15×10^{-2}
path:rno04912	GnRH signaling pathway	1.30×10^{-2}	7.78×10^{-2}

Table 2 | Cellular functional pathways in which the differentially phosphorylated proteins were significantly over-represented.

KEGG pathway	Pathway name	Raw *p* value	*FDR*
path:rno04530	Tight junction	2.12×10^{-9}	2.41×10^{-7}
path:rno03040	Spliceosome	7.64×10^{-7}	2.85×10^{-5}
path:rno04211	Longevity regulating pathway	7.61×10^{-5}	1.16×10^{-3}
path:rno03013	RNA transport	7.17×10^{-5}	1.16×10^{-3}
path:rno04213	Longevity regulating pathway - multiple species	1.30×10^{-4}	1.77×10^{-3}
path:rno04520	Adherens junction	5.45×10^{-4}	4.92×10^{-3}
path:rno04510	Focal adhesion	5.07×10^{-4}	4.92×10^{-3}
path:rno04210	Apoptosis	4.43×10^{-3}	3.15×10^{-2}
path:rno04070	Phosphatidylinositol signaling system	6.94×10^{-3}	4.72×10^{-2}
path:rno04540	Gap junction	8.20×10^{-3}	5.33×10^{-2}
path:rno04810	Regulation of actin cytoskeleton	1.19×10^{-2}	7.40×10^{-2}

Table 3 | Averages and Medians of EC_{50} and $T_{1/2}$ values in DEGs

		Average	Median	*p* value	Adjusted *p* value
EC_{50} (nM)	Up-regulated	1.55	2.19	9.64×10^{-15}	3.86×10^{-14}
	Down-regulated	0.25	0.16		
$T_{1/2}$ (min)	Up-regulated	67.56	50.15	9.82×10^{-5}	3.93×10^{-4}
	Down-regulated	86.86	58.51		

Table 4 | Averages and Medians of EC_{50} and $T_{1/2}$ values in DCMs

		Average	Median	*p* value	Adjusted *p* value
EC_{50} (nM)	Increased	4.90	6.61	1.34×10^{-10}	5.36×10^{-10}
	Decreased	1.29	1.23		
$T_{1/2}$ (min)	Increased	56.14	67.93	1.90×10^{-3}	7.60×10^{-3}
	Decreased	17.97	10.93		

Table 5 | Antibodies used in the western blotting analysis

Antibodies	Source	Identifier
Anti-pIrs Tyr612	Abcam	Cat#ab66153; RRID:AB_1140753
Anti-pIrs Tyr632	Santa Cruz	Cat#SC17196; RRID:AB_669445
Anti-pAkt Ser473	CST	Cat#4060; RRID:AB_2315049
Anti-pAkt Thr308	CST	Cat#9275; RRID:AB_329828
Anti-pS6k Thr389	CST	Cat#9205; RRID:AB_330944
Anti-pGsk3β Ser9	CST	Cat#9336; RRID:AB_331405
Anti-pErk1/2 Thr202/Tyr204	CST	Cat#9101; RRID:AB_331646
Anti-pp38 Thr180/Tyr182	CST	Cat#9211; RRID:AB_331641
Anti-pSapk/Jnk Thr183/Tyr185	CST	Cat#4668; RRID:AB_2307320
Anti-pAmpkα Thr172	CST	Cat#2531; RRID:AB_330330
Anti-pTsc2 Thr1462	CST	Cat#3617; RRID:AB_490956
Anti-pFoxo1 Ser256	CST	Cat#9461; RRID:AB_329831
Anti-pCreb Ser133	CST	Cat#9191; RRID:AB_331606
Anti-pAtf2 Thr71	CST	Cat#9221; RRID:AB_2561045
Anti-pc-Jun Ser73	CST	Cat#3270; RRID:AB_2129572
Anti-Egr1	CST	Cat#4154; RRID:AB_2097035
Anti-c-Jun	CST	Cat#9165; RRID:AB_2130165
Anti-HES1	CST	Cat#11988
Anti-pS6 Ser235/236	CST	Cat#2211; RRID:AB_331679
Anti-p4eIf4ebp1 Ser65	CST	Cat#9451; RRID:AB_330947
Anti-peIf4b Ser422	CST	Cat#3591; RRID:AB_10080112
Anti-Rabbit IgG, Peroxidase-conjugated	GE Healthcare	Cat#NA9340V; RRID:AB_772206
Anti-Mouse IgG, Peroxidase-conjugated	GE Healthcare	Cat#NXA931; RRID:AB_772209
Anti-Goat IgG, Peroxidase-conjugated	Sigma-Aldrich	Cat#A-5420; RRID:AB_258242

8. Supplemental Tables

All of the Supplemental tables in *.xlsx format is also downloadable from our website (http://kurodalab.bs.s.u-tokyo.ac.jp/Doctoral/Kawata/). These *.xlsx files can be opened with Microsoft Excel.

Table S1 | Pathway over-representation analysis.

Table S2 | The pathways that work in specific tissues other than liver.

Table S3 | List of the kinases in the kinase classifiers defined in NetPhorest.

Table S4 | Prediction of responsible protein kinases.

Table S5 | Occurrence rates of kinase classifiers in each pathway.

Table S6 | Classification of DEGs according to EC_{50} and $T_{1/2}$ values.

Table S7 | Prediction of TFs for each class of DEGs.

Table S8 | Regulators of the TFs estimated for the DEGs identified from KEGG.

Table S9 | Time series of metabolome data in response to insulin stimulation.

Table S10 | Classification of DCMs according to EC_{50} and $T_{1/2}$ values.

Table S11 | Identification of RMEs regulating the DCMs.

Table S12 | Identification of allosteric regulators of the RMEs.

Table S13 | Classification of signaling molecules according to EC_{50} and $T_{1/2}$ values.

9. References

1. Zimmet P, Alberti KGMM, Shaw J. Global and societal implications of the diabetes epidemic. Nature. 2001;414: 782–787. doi:10.1038/414782a

2. Whiteman EL, Cho H, Birnbaum MJ. Role of Akt/protein kinase B in metabolism. Trends Endocrinol Metab. 2002;13: 444–51. Available: http://www.ncbi.nlm.nih.gov/pubmed/12431841

3. Saltiel AR, Kahn CR. Insulin signalling and the regulation of glucose and lipid metabolism. Nature. 2001;414: 799–806. doi:10.1038/414799a

4. Jastrzebski K, Hannan KM, Tchoubrieva EB, Hannan RD, Pearson RB. Coordinate regulation of ribosome biogenesis and function by the ribosomal protein S6 kinase, a key mediator of mTOR function. Growth Factors. 2007;25: 209–226. doi:10.1080/08977190701779101

5. Lizcano JM, Alessi DR. The insulin signalling pathway. Curr Biol. 2002;12: R236-8. Available: http://www.ncbi.nlm.nih.gov/pubmed/11937037

6. Asnaghi L, Bruno P, Priulla M, Nicolin A. mTOR: a protein kinase switching between life and death. Pharmacol Res. 2004;50: 545–9. doi:10.1016/j.phrs.2004.03.007

7. Kotzka J, Lehr S, Roth G, Avci H, Knebel B, Muller-Wieland D. Insulin-activated Erk-mitogen-activated protein kinases phosphorylate sterol regulatory element-binding Protein-2 at serine residues 432 and 455 in vivo. J Biol Chem. American Society for Biochemistry and Molecular Biology; 2004;279: 22404–11. doi:10.1074/jbc.M401198200

8. Zhang W, Thompson BJ, Hietakangas V, Cohen SM. MAPK/ERK Signaling Regulates Insulin Sensitivity to Control Glucose Metabolism in Drosophila. Rulifson E, editor. PLoS Genet. 2011;7: e1002429. doi:10.1371/journal.pgen.1002429

9. Mounier C, Posner BI. Transcriptional regulation by insulin: from the receptor to the geneThis paper is one of a selection of papers published in this Special issue, entitled Second Messengers and Phosphoproteins—12th International Conference. Can J Physiol Pharmacol. 2006;84: 713–724. doi:10.1139/y05-152

10. Barthel A, Schmoll D, Unterman TG. FoxO proteins in insulin action and metabolism. Trends Endocrinol Metab. 2005;16: 183–9. doi:10.1016/j.tem.2005.03.010

11. Au W-S, Kung H, Lin MC. Regulation of microsomal triglyceride transfer protein gene by insulin in HepG2 cells: roles of MAPKerk and MAPKp38. Diabetes. 2003;52: 1073–80. Available: http://www.ncbi.nlm.nih.gov/pubmed/12716735

12. Biggs WH, Meisenhelder J, Hunter T, Cavenee WK, Arden KC. Protein kinase B/Akt-mediated phosphorylation promotes nuclear exclusion of the winged helix transcription factor FKHR1. Proc Natl Acad Sci U S A. 1999;96: 7421–6. Available: http://www.ncbi.nlm.nih.gov/pubmed/10377430

13. Brunet A, Bonni A, Zigmond MJ, Lin MZ, Juo P, Hu LS, et al. Akt promotes cell survival by phosphorylating and inhibiting a Forkhead transcription factor. Cell. 1999;96: 857–68. Available: http://www.ncbi.nlm.nih.gov/pubmed/10102273

14. Lu M, Wan M, Leavens KF, Chu Q, Monks BR, Fernandez S, et al. Insulin regulates liver metabolism in vivo in the absence of hepatic Akt and Foxo1. Nat Med. 2012;18: 388–395. doi:10.1038/nm.2686

15. Nakayama K, Satoh T, Igari A, Kageyama R, Nishida E. FGF induces oscillations of Hes1 expression and Ras/ERK activation. Curr Biol. 2008;18: R332-4. doi:10.1016/j.cub.2008.03.013

16. Shaul YD, Seger R. The MEK/ERK cascade: From signaling specificity to diverse functions. Biochim Biophys Acta - Mol Cell Res. 2007;1773: 1213–1226. doi:10.1016/j.bbamcr.2006.10.005

17. Murphy LO, MacKeigan JP, Blenis J. A network of immediate early gene products propagates subtle differences in mitogen-activated protein kinase signal amplitude and duration. Mol Cell Biol. 2004;24: 144–53. Available: http://www.ncbi.nlm.nih.gov/pubmed/14673150

18. Deak M, Clifton AD, Lucocq LM, Alessi DR. Mitogen- and stress-activated protein kinase-1 (MSK1) is directly activated by MAPK and SAPK2/p38, and may mediate activation of CREB. EMBO J. 1998;17: 4426–41. doi:10.1093/emboj/17.15.4426

19. Lee YH, Giraud J, Davis RJ, White MF. c-Jun N-terminal kinase (JNK) mediates feedback inhibition of the insulin signaling cascade. J Biol Chem. American Society for Biochemistry and Molecular Biology; 2003;278: 2896–902. doi:10.1074/jbc.M208359200

20. Fukunaga K, Noguchi T, Takeda H, Matozaki T, Hayashi Y, Itoh H, et al. Requirement for protein-tyrosine phosphatase SHP-2 in insulin-induced activation of

c-Jun NH(2)-terminal kinase. J Biol Chem. American Society for Biochemistry and Molecular Biology; 2000;275: 5208–13. doi:10.1074/JBC.275.7.5208

21. Rosner M, Siegel N, Valli A, Fuchs C, Hengstschl?ger M. mTOR phosphorylated at S2448 binds to raptor and rictor. Amino Acids. Springer Vienna; 2010;38: 223–228. doi:10.1007/s00726-008-0230-7

22. Humphrey S, Yang G, Yang P, Fazakerley D, St?ckli J, Yang J, et al. Dynamic Adipocyte Phosphoproteome Reveals that Akt Directly Regulates mTORC2. Cell Metab. 2013;17: 1009–1020. doi:10.1016/j.cmet.2013.04.010

23. Tsakiridis T, Tong P, Matthews B, Tsiani E, Bilan PJ, Klip A, et al. Role of the actin cytoskeleton in insulin action. Microsc Res Tech. 1999;47: 79–92. doi:10.1002/(SICI)1097-0029(19991015)47:2<79::AID-JEMT1>3.0.CO;2-S

24. Wolf A, Rietscher K, Glaß M, Hüttelmaier S, Schutkowski M, Ihling C, et al. Insulin signaling via Akt2 switches plakophilin 1 function from stabilizing cell adhesion to promoting cell proliferation. J Cell Sci. 2013;126: 1832–44. doi:10.1242/jcs.118992

25. Reiss K, Wang JY, Romano G, Tu X, Peruzzi F, Baserga R. Mechanisms of regulation of cell adhesion and motility by insulin receptor substrate-1 in prostate cancer cells. Oncogene. 2001;20: 490–500. doi:10.1038/sj.onc.1204112

26. Hartmann B, Castelo R, Blanchette M, Boue S, Rio DC, Valcárcel J. Global analysis of alternative splicing regulation by insulin and wingless signaling in Drosophila cells. Genome Biol. 2009;10: R11. doi:10.1186/gb-2009-10-1-r11

27. Friedman AA, Tucker G, Singh R, Yan D, Vinayagam A, Hu Y, et al. Proteomic and Functional Genomic Landscape of Receptor Tyrosine Kinase and Ras to Extracellular Signal-Regulated Kinase Signaling. Sci Signal. 2011;4: rs10-rs10. doi:10.1126/scisignal.2002029

28. Vinayagam A, Kulkarni MM, Sopko R, Sun X, Hu Y, Nand A, et al. An Integrative Analysis of the InR/PI3K/Akt Network Identifies the Dynamic Response to Insulin Signaling. Cell Rep. 2016;16: 3062–74. doi:10.1016/j.celrep.2016.08.029

29. Monetti M, Nagaraj N, Sharma K, Mann M. Large-scale phosphosite quantification in tissues by a spike-in SILAC method. Nat Methods. 2011;8: 655–8. doi:10.1038/nmeth.1647

30. Zhang Y, Zhang Y, Yu Y. Global Phosphoproteomic Analysis of Insulin/Akt/mTORC1/S6K Signaling in Rat Hepatocytes. J Proteome Res. 2017; acs.jproteome.7b00140. doi:10.1021/acs.jproteome.7b00140

31. Krüger M, Kratchmarova I, Blagoev B, Tseng Y-H, Kahn CR, Mann M. Dissection of the insulin signaling pathway via quantitative phosphoproteomics. Proc Natl Acad Sci U S A. 2008;105: 2451–6. doi:10.1073/pnas.0711713105

32. Yugi K, Kubota H, Toyoshima Y, Noguchi R, Kawata K, Komori Y, et al. Reconstruction of Insulin Signal Flow from Phosphoproteome and Metabolome Data. Cell Rep. 2014;8: 1171–1183. doi:10.1016/j.celrep.2014.07.021

33. Hectors TLM, Vanparys C, Pereira-Fernandes A, Knapen D, Blust R. Mechanistic evaluation of the insulin response in H4IIE hepatoma cells: New endpoints for toxicity testing? Toxicol Lett. 2012;212: 180–189. doi:10.1016/j.toxlet.2012.05.016

34. Dupont J, Khan J, Qu B-H, Metzler P, Helman L, LeRoith D. Insulin and IGF-1 Induce Different Patterns of Gene Expression in Mouse Fibroblast NIH-3T3 Cells: Identification by cDNA Microarray Analysis. Endocrinology. 2001;142: 4969–4975. doi:10.1210/endo.142.11.8476

35. Versteyhe S, Klaproth B, Borup R, Palsgaard J, Jensen M, Gray SG, et al. IGF-I, IGF-II, and Insulin Stimulate Different Gene Expression Responses through Binding to the IGF-I Receptor. Front Endocrinol (Lausanne). 2013;4: 98. doi:10.3389/fendo.2013.00098

36. Kim HS, Lee NK. Gene expression profiling in osteoclast precursors by insulin using microarray analysis. Mol Cells. 2014;37: 827–32. doi:10.14348/molcells.2014.0223

37. Rome S, Clément K, Rabasa-Lhoret R, Loizon E, Poitou C, Barsh GS, et al. Microarray profiling of human skeletal muscle reveals that insulin regulates approximately 800 genes during a hyperinsulinemic clamp. J Biol Chem. 2003;278: 18063–8. doi:10.1074/jbc.M300293200

38. Sano T, Kawata K, Ohno S, Yugi K, Kakuda H, Kubota H, et al. Selective control of up-regulated and down-regulated genes by temporal patterns and doses of insulin. Sci Signal. 2016;112: 1–12. doi:10.1126/scisignal.aaf3739

39. Newgard CB, An J, Bain JR, Muehlbauer MJ, Stevens RD, Lien LF, et al. A Branched-Chain Amino Acid-Related Metabolic Signature that Differentiates Obese and Lean Humans and Contributes to Insulin Resistance. Cell Metab. 2009;9: 311–326. doi:10.1016/j.cmet.2009.02.002

40. Everman S, Meyer C, Tran L, Hoffman N, Carroll CC, Dedmon WL, et al. Insulin does not stimulate muscle protein synthesis during increased plasma branched-chain amino acids alone but still decreases whole body proteolysis in humans. Am J Physiol Endocrinol Metab. 2016;311: E671–E677. doi:10.1152/ajpendo.00120.2016

41. Noguchi R, Kubota H, Yugi K, Toyoshima Y, Komori Y, Soga T, et al. The selective control of glycolysis, gluconeogenesis and glycogenesis by temporal insulin patterns. Mol Syst Biol. 2013;9: 664. doi:10.1038/msb.2013.19

42. Buescher JM, Liebermeister W, Jules M, Uhr M, Muntel J, Botella E, et al. Global Network Reorganization During Dynamic Adaptations of Bacillus subtilis Metabolism. Science (80-). 2012;335: 1099–1103. doi:10.1126/science.1206871

43. Palsson B, Zengler K. The challenges of integrating multi-omic data sets. Nat Chem Biol. 2010;6: 787–9. Available: http://www.ncbi.nlm.nih.gov/pubmed/20976870

44. Joyce AR, Palsson BØ. The model organism as a system: integrating “omics” data sets. Nat Rev Mol Cell Biol. 2006;7: 198–210. doi:10.1038/nrm1857

45. Hatzimanikatis V, Saez-Rodriguez J. Integrative approaches for signalling and metabolic networks. Integr Biol (Camb). 2015;7: 844–5. doi:10.1039/c5ib90030a

46. Hyduke DR, Lewis NE, Palsson BØ. Analysis of omics data with genome-scale models of metabolism. Mol Biosyst. NIH Public Access; 2013;9: 167–74. doi:10.1039/c2mb25453k

47. Yugi K, Kuroda S. Metabolism-Centric Trans-Omics. Cell Syst. 2017;4: 19–20. doi:10.1016/j.cels.2017.01.007

48. Yugi K, Kubota H, Hatano A, Kuroda S. Trans-Omics: How To Reconstruct Biochemical Networks Across Multiple ?Omic? Layers. Trends Biotechnol. 2016;34: 276–290. doi:10.1016/j.tibtech.2015.12.013

49. Ishii N, Nakahigashi K, Baba T, Robert M, Soga T, Kanai A, et al. Multiple high-throughput analyses monitor the response of E. coli to perturbations. Science. 2007;316: 593–7. doi:10.1126/science.1132067

50. Gerosa L, Haverkorn van Rijsewijk BRB, Christodoulou D, Kochanowski K, Schmidt TSB, Noor E, et al. Pseudo-transition Analysis Identifies the Key Regulators of Dynamic Metabolic Adaptations from Steady-State Data. Cell Syst. 2015;1: 270–282. doi:10.1016/j.cels.2015.09.008

51. Oliveira AP, Ludwig C, Picotti P, Kogadeeva M, Aebersold R, Sauer U. Regulation of yeast central metabolism by enzyme phosphorylation. Mol Syst Biol. 2012;8: 623. doi:10.1038/msb.2012.55

52. Hackett SR, Zanotelli VRT, Xu W, Goya J, Park JO, Perlman DH, et al. Systems-level analysis of mechanisms regulating yeast metabolic flux. Science (80-). 2016;354: aaf2786-aaf2786. doi:10.1126/science.aaf2786

53. Gonçalves E, Raguz Nakic Z, Zampieri M, Wagih O, Ochoa D, Sauer U, et al. Systematic Analysis of Transcriptional and Post-transcriptional Regulation of Metabolism in Yeast. Patil KR, editor. PLOS Comput Biol. 2017;13: e1005297. doi:10.1371/journal.pcbi.1005297

54. Yusufi FNK, Lakshmanan M, Ho YS, Loo BLW, Ariyaratne P, Yang Y, et al. Mammalian Systems Biotechnology Reveals Global Cellular Adaptations in a Recombinant CHO Cell Line. Cell Syst. 2017;4: 530–542.e6. doi:10.1016/j.cels.2017.04.009

55. Geiger R, Rieckmann JC, Wolf T, Basso C, Feng Y, Fuhrer T, et al. L-Arginine Modulates T Cell Metabolism and Enhances Survival and Anti-tumor Activity. Cell. 2016;167: 829–842.e13. doi:10.1016/j.cell.2016.09.031

56. Behar M, Hoffmann A. Understanding the temporal codes of intra-cellular signals. Curr Opin Genet Dev. 2010;20: 684–93. doi:10.1016/j.gde.2010.09.007

57. Polonsky KS, Given BD, Van Cauter E. Twenty-four-hour profiles and pulsatile patterns of insulin secretion in normal and obese subjects. J Clin Invest. 1988;81: 442–448. doi:10.1172/JCI113339

58. Lindsay JR, McKillop AM, Mooney MH, Flatt PR, Bell PM, O'Harte FPM. Meal-induced 24-hour profile of circulating glycated insulin in type 2 diabetic subjects measured by a novel radioimmunoassay. Metabolism. 2003;52: 631–635. doi:10.1053/meta.2003.50150

59. Kubota H, Noguchi R, Toyoshima Y, Ozaki Y, Uda S, Watanabe K, et al. Temporal Coding of Insulin Action through Multiplexing of the AKT Pathway. Mol Cell. 2012;46: 820–832. doi:10.1016/j.molcel.2012.04.018

60. Humphrey SJ, Azimifar SB, Mann M. High-throughput phosphoproteomics reveals in vivo insulin signaling dynamics. Nat Biotechnol. 2015;33: 990–5. doi:10.1038/nbt.3327

61. Olsen J V, Vermeulen M, Santamaria A, Kumar C, Miller ML, Jensen LJ, et al. Quantitative phosphoproteomics reveals widespread full phosphorylation site occupancy during mitosis. Sci Signal. 2010;3: ra3. doi:10.1126/scisignal.2000475

62. Olsen J V, Blagoev B, Gnad F, Macek B, Kumar C, Mortensen P, et al. Global, in vivo, and site-specific phosphorylation dynamics in signaling networks. Cell. 2006;127: 635–48. doi:10.1016/j.cell.2006.09.026

63. Horn H, Schoof EM, Kim J, Robin X, Miller ML, Diella F, et al. KinomeXplorer: an integrated platform for kinome biology studies. Nat Methods. 2014;11: 603–4. doi:10.1038/nmeth.2968

64. Miller ML, Jensen LJ, Diella F, Jorgensen C, Tinti M, Li L, et al. Linear Motif Atlas for Phosphorylation-Dependent Signaling. Sci Signal. 2008;1: ra2-ra2. doi:10.1126/scisignal.1159433

65. Workman CT, Yin Y, Corcoran DL, Ideker T, Stormo GD, Benos P V. enoLOGOS: a versatile web tool for energy normalized sequence logos. Nucleic Acids Res. 2005;33: W389-92. doi:10.1093/nar/gki439

66. Colaert N, Helsens K, Martens L, Vandekerckhove J, Gevaert K. Improved visualization of protein consensus sequences by iceLogo. Nat Methods. 2009;6: 786–787. doi:10.1038/nmeth1109-786

67. Matys V, Kel-Margoulis O V, Fricke E, Liebich I, Land S, Barre-Dirrie A, et al. TRANSFAC(R) and its module TRANSCompel(R): transcriptional gene regulation in eukaryotes. Nucleic Acids Res. 2006;34: D108–D110. doi:10.1093/nar/gkj143

68. Kel AE, Gössling E, Reuter I, Cheremushkin E, Kel-Margoulis O V, Wingender E. MATCH: A tool for searching transcription factor binding sites in DNA sequences.

Nucleic Acids Res. 2003;31: 3576–9. Available: http://www.ncbi.nlm.nih.gov/pubmed/12824369

69. Matsuzaki H, Daitoku H, Hatta M, Tanaka K, Fukamizu A. Insulin-induced phosphorylation of FKHR (Foxo1) targets to proteasomal degradation. Proc Natl Acad Sci U S A. 2003;100: 11285–90. doi:10.1073/pnas.1934283100

70. Puigserver P, Rhee J, Donovan J, Walkey CJ, Yoon JC, Oriente F, et al. Insulin-regulated hepatic gluconeogenesis through FOXO1-PGC-1alpha interaction. Nature. 2003;423: 550–5. doi:10.1038/nature01667

71. Schomburg I, Chang A, Placzek S, Söhngen C, Rother M, Lang M, et al. BRENDA in 2013: integrated reactions, kinetic data, enzyme function data, improved disease classification: new options and contents in BRENDA. Nucleic Acids Res. 2013;41: D764-72. doi:10.1093/nar/gks1049

72. Thiel G, Cibelli G. Regulation of life and death by the zinc finger transcription factor Egr-1. J Cell Physiol. 2002;193: 287–292. doi:10.1002/jcp.10178

73. Sukhatme VP, Cao XM, Chang LC, Tsai-Morris CH, Stamenkovich D, Ferreira PC, et al. A zinc finger-encoding gene coregulated with c-fos during growth and

differentiation, and after cellular depolarization. Cell. 1988;53: 37–43. Available: http://www.ncbi.nlm.nih.gov/pubmed/3127059

74. Herzig S, Hedrick S, Morantte I, Koo S-H, Galimi F, Montminy M. CREB controls hepatic lipid metabolism through nuclear hormone receptor PPAR-γ. Nature. 2003;426: 190–193. doi:10.1038/nature02110

75. Lemke U, Krones-Herzig A, Diaz MB, Narvekar P, Ziegler A, Vegiopoulos A, et al. The Glucocorticoid Receptor Controls Hepatic Dyslipidemia through Hes1. Cell Metab. 2008;8: 212–223. doi:10.1016/j.cmet.2008.08.001

76. Durr IF, Rudney H. The reduction of beta-hydroxy-beta-methyl-glutaryl coenzyme A to mevalonic acid. J Biol Chem. 1960;235: 2572–8. Available: http://www.ncbi.nlm.nih.gov/pubmed/13818862

77. Lindgren V, Luskey KL, Russell DW, Francke U. Human genes involved in cholesterol metabolism: chromosomal mapping of the loci for the low density lipoprotein receptor and 3-hydroxy-3-methylglutaryl-coenzyme A reductase with cDNA probes. Proc Natl Acad Sci U S A. 1985;82: 8567–71. Available: http://www.ncbi.nlm.nih.gov/pubmed/3866240

78. Oliveira AP, Ludwig C, Zampieri M, Weisser H, Aebersold R, Sauer U. Dynamic phosphoproteomics reveals TORC1-dependent regulation of yeast nucleotide and amino acid biosynthesis. Sci Signal. 2015;8: rs4. doi:10.1126/scisignal.2005768

79. Shyh-Chang N, Locasale JW, Lyssiotis CA, Zheng Y, Teo RY, Ratanasirintrawoot S, et al. Influence of threonine metabolism on S-adenosylmethionine and histone methylation. Science. 2013;339: 222–6. doi:10.1126/science.1226603

80. Ota K, Feng S-Y, Ito T. Detecting protein-DNA interactions using a modified yeast one-hybrid system. Methods Mol Biol. 2014;1164: 39–50. doi:10.1007/978-1-4939-0805-9_5

81. Colicchio JM, Miura F, Kelly JK, Ito T, Hileman LC. DNA methylation and gene expression in Mimulus guttatus. BMC Genomics. 2015;16: 507. doi:10.1186/s12864-015-1668-0

82. Kanehisa M, Goto S, Sato Y, Furumichi M, Tanabe M. KEGG for integration and interpretation of large-scale molecular data sets. Nucleic Acids Res. 2012;40: D109-14. doi:10.1093/nar/gkr988

83. Kanehisa M, Furumichi M, Tanabe M, Sato Y, Morishima K. KEGG: new perspectives on genomes, pathways, diseases and drugs. Nucleic Acids Res. 2017;45: D353–D361. doi:10.1093/nar/gkw1092

84. Fisher RA. On the Interpretation of χ 2 from Contingency Tables, and the Calculation of P. J R Stat Soc. 1922;85: 87. doi:10.2307/2340521

85. Storey JD, Taylor JE, Siegmund D. Strong control, conservative point estimation and simultaneous conservative consistency of false discovery rates: a unified approach. J R Stat Soc Ser B (Statistical Methodol. Blackwell Publishing; 2004;66: 187–205. doi:10.1111/j.1467-9868.2004.00439.x

86. Kersey PJ, Duarte J, Williams A, Karavidopoulou Y, Birney E, Apweiler R. The International Protein Index: An integrated database for proteomics experiments. Proteomics. 2004;4: 1985–1988. doi:10.1002/pmic.200300721

87. Ward JH. Hierarchical Grouping to Optimize an Objective Function. J Am Stat Assoc. 1963;58: 236–244. doi:10.1080/01621459.1963.10500845

88. Trapnell C, Pachter L, Salzberg SL. TopHat: discovering splice junctions with RNA-Seq. Bioinformatics. 2009;25: 1105–11. doi:10.1093/bioinformatics/btp120

89. Kim D, Pertea G, Trapnell C, Pimentel H, Kelley R, Salzberg SL. TopHat2: accurate alignment of transcriptomes in the presence of insertions, deletions and gene fusions. Genome Biol. 2013;14: R36. doi:10.1186/gb-2013-14-4-r36

90. Trapnell C, Roberts A, Goff L, Pertea G, Kim D, Kelley DR, et al. Differential gene and transcript expression analysis of RNA-seq experiments with TopHat and Cufflinks. Nat Protoc. 2012;7: 562–578. doi:10.1038/nprot.2012.016

91. Hollander M, A. Wolfe D, Chicken E. Nonparametric Statistical Methods [Internet]. Nonparametric Statistical Methods. Hoboken, NJ, USA: John Wiley & Sons, Inc.; 2015. doi:10.1002/9781119196037.ch1

92. Gibbons JD, Chakraborti S. Nonparametric statistical inference [Internet]. Chapman & Hall/Taylor & Francis; 2011. Available: https://www.crcpress.com/Nonparametric-Statistical-Inference-Fifth-Edition/Gibbons-Chakraborti/p/book/9781420077612

93. Bonferroni. Teoria statistica delle classi e calcolo delle probabilit¥`{a}. Pubbl del R Ist Super di Sci Econ e Commer di Firenze. 1936;8. Available: http://www.citeulike.org/user/barriot/article/1778138

94. Otsu N. A Threshold Selection Method from Gray-Level Histograms. IEEE Trans Syst Man Cybern. 1979;9: 62–66. doi:10.1109/TSMC.1979.4310076

95. Kinsella RJ, Kahari A, Haider S, Zamora J, Proctor G, Spudich G, et al. Ensembl BioMarts: a hub for data retrieval across taxonomic space. Database. 2011;2011: bar030-bar030. doi:10.1093/database/bar030

96. Arner E, Daub CO, Vitting-Seerup K, Andersson R, Lilje B, Drabløs F, et al. Transcribed enhancers lead waves of coordinated transcription in transitioning mammalian cells. Science. 2015;347: 1010–4. doi:10.1126/science.1259418

97. Mudunuri U, Che A, Yi M, Stephens RM. bioDBnet: the biological database network. Bioinformatics. 2009;25: 555–6. doi:10.1093/bioinformatics/btn654

98. Lange AJ, Argaud D, el-Maghrabi MR, Pan W, Maitra SR, Pilkis SJ. Isolation of a cDNA for the catalytic subunit of rat liver glucose-6-phosphatase: regulation of gene expression in FAO hepatoma cells by insulin, dexamethasone and cAMP. Biochem Biophys Res Commun. 1994;201: 302–9. Available: http://www.ncbi.nlm.nih.gov/pubmed/8198588

99. Soga T, Baran R, Suematsu M, Ueno Y, Ikeda S, Sakurakawa T, et al. Differential metabolomics reveals ophthalmic acid as an oxidative stress biomarker indicating

hepatic glutathione consumption. J Biol Chem. 2006;281: 16768–76. doi:10.1074/jbc.M601876200

100. Soga T, Igarashi K, Ito C, Mizobuchi K, Zimmermann H-P, Tomita M. Metabolomic Profiling of Anionic Metabolites by Capillary Electrophoresis Mass Spectrometry. Anal Chem. 2009;81: 6165–6174. doi:10.1021/ac900675k

101. Alves R, Chaleil RAG, Sternberg MJE. Evolution of enzymes in metabolism: a network perspective. J Mol Biol. 2002;320: 751–70. Available: http://www.ncbi.nlm.nih.gov/pubmed/12095253

10. Acknowledgments

I am full of gratitude to a lot of people who supported this study. I thank Prof. Shinya Kuroda for teaching principles of scientific research. I also thank Prof. Keiich I. Nakayama and Prof. Masaki Matsumoto (of Medical Institute of Bioregulation, Kyushu University), Prof. Yutaka Suzuki (of Graduate School of Frontier Sciences, University of Tokyo), and Prof. Tomoyoshi Soga (of the Institute for Advanced Biosciences, Keio University) for providing excellent technical support for the phosphoproteome, the transcriptome, and the metabolome measurement, respectively. I thank the other authors and all member of Kuroda laboratory for their critical reading of this manuscript, helpful discussions, and technical assistance with the experiments.

This work was financially supported by the Creation of Fundamental Technologies for Understanding and Control of Biosystem Dynamics, CREST (JPMJCR12W3) from the Japan Science and Technology Agency (JST), and by the Japan Society for the Promotion of Science (JSPS) KAKENHI Grant Number (17H06300, 17H06299).

Finally, I would like to express my gratitude to my friends and family for their supports. Especially, I sincerely thank to my wife, Yumiko, for her warm encouragement.